

ACKNOWLEDGEMENTS

TODO: Thanks to everyone...

TABLE OF CONTENTS

 1
	Page
1. INTRODUCTION	6
1.1 QUANTUM PHYSICS AND THE STANDARD MODEL IN A NUT-SHELL	6
1.2 THE TROUBLE WITH UNDERSTANDING THE NUCLEON	9
1.3 SCATTERING EXPERIMENTS AND BONUS12	10
1.4 INCLUSIVE DEEP INELASTIC SCATTERING DATA ANALYSIS ON RUN GROUP A DATA	10
2. PHYSICS FORMALISM	12
2.1 NUCLEON STRUCTURE	12
2.2 ELECTRON-SCATTERING KINEMATICS	14
2.3 ELASTIC SCATTERING	19
2.4 RESONANCE REGION	23
2.5 DEEP INELASTIC SCATTERING	24
2.6 PARTONS AND BJORKEN-SCALING	25
2.7 NUCLEON STRUCTURE-FUNCTION RATIO F_N^2/F_P^2	28
2.8 DIFFICULTIES IN EXTRACTING F_N^2/F_P^2 FROM DEUTERIUM ..	29
2.8.1 BOUND NUCLEON STRUCTURE	29
2.8.2 BACKGROUNDS	29
2.9 BARELY OFF-SHELL NUCLEON STRUCTURE	29
3. THE BONUS12 EXPERIMENT	30
3.1 CONTINUOUS ELECTRON BEAM ACCELERATOR FACILITY ..	30
3.2 CEBAF LARGE ACCEPTANCE SPECTROMETER	31
3.2.1 TORUS MAGNET	32
3.2.2 CHERENKOV COUNTERS	33
3.2.3 DRIFT CHAMBERS	34
3.2.4 FORWARD TIME OF FLIGHT	34
3.2.5 ELECTROMAGNETIC CALORIMETER	35

3.2.6	SOLENOID MAGNET	36
3.2.7	CENTRAL TIME OF FLIGHT	36
3.3	BONUS12 RTPC	36
3.3.1	COMPONENTS AND THEIR PURPOSE.....	37
3.3.2	BONUS12 RTPC DRIFT-GAS MONITORING SYSTEM	39
3.3.3	CONSTRUCTION AND INTEGRATION	41
4.	SIMULATION AND DEVELOPMENT	43
4.1	GEANT4 MONTE CARLO (GEMC)	43
4.2	GARFIELD++	44
4.3	BONUS12 RTPC SIMULATIONS	44
4.3.1	GEOMETRY & MATERIALS	45
4.3.2	EVENT GENERATOR	47
4.3.3	DRIFT ELECTRONS	49
4.3.4	GAS OPTIMIZATION.....	51
4.3.5	DRIFT EQUATIONS.....	55
4.4	DMS SIMULATIONS	57
4.4.1	GEOMETRY	57
4.4.2	ELECTRIC FIELD	59
4.4.3	DRIFT VELOCITY	61
5.	DATA ANALYSIS	63
5.1	ELECTRON RECONSTRUCTION	63
5.2	PROTON RECONSTRUCTION	63
5.3	HELIX FITTER AND KALMAN FILTER.....	63
5.4	CALIBRATION	63
5.5	CUTS AND CORRECTIONS	63
5.6	KINEMATIC COVERAGE AND DATA BINNING	63
5.7	ACCEPTANCE CORRECTION	63
5.8	ELECTRON DETECTION EFFICIENCY.....	63
5.9	BACKGROUND SUBTRACTION	63
5.10	CROSS SECTION CALCULATION	63
5.11	RADIATIVE CORRECTIONS	63
5.12	SYSTEMATIC ERROR EVALUATION	63

6. RESULTS.....	64
-----------------	----

APPENDICES

VITA.....	66
-----------	----

CHAPTER 1

INTRODUCTION

Throughout human history we have been driven to understand the world around us. It is surely one of the characteristics that defines us as a species. Coupling that curiosity with our ability to create and construct incredible machines has allowed us to probe some of the most elusive parts of our Universe. From the Hubble Telescope taking images of the earliest moments of our Universe to the Large Hadron Collider probing the most fundamental particles that we currently know, we have been wildly successful at fulfilling that drive to understand.

Despite that success, there are many issues that continue to elude us. Dark matter and dark energy, which are collectively believed to make up 96% of our Universe, are phenomena we know almost nothing about. Another puzzle that we currently have no tangible explanation for is the asymmetry of matter to anti-matter. In the very early Universe there were equal amounts of matter and anti-matter, yet today our visible Universe seems to be comprised primarily of matter and not anti-matter. Even of the matter that we do know of, we know surprisingly little about its structure and composition.

Atoms make up much of that visible Universe. Since the early 1900's we have known these atoms to be made of protons, neutrons and electrons. The discovery of protons and electrons essentially occurred in the late 19th Century, but the neutron was not discovered until 1932 by Sir James Chadwick. The neutron was not just found later than the electron and proton, but we also know much less about it. The electron is well-known in the physics community to be a near point-like particle made of no constituent particles, but the proton and neutron have been proven to be made of more fundamental particles.

1.1 QUANTUM PHYSICS AND THE STANDARD MODEL IN A NUTSHELL

Knowing exactly what makes up these protons and neutrons relies on knowledge of the Standard Model of Particle Physics, or sometimes referred to as just the Standard Model. This model, developed in stages throughout the latter half of the

20th Century, essentially lays out the existence of all possible fundamental¹ particles in the Universe.

There are 17 particles in the Standard Model (outlined in Fig. 1). These 17 can first be broken down into two subgroups called bosons and fermions. Bosons follow what is known as Bose-Einstein statistics, which essentially states that they can occupy the same space at the same time. In the language of quantum physics, two bosons can be described by the same quantum numbers. These bosons, with a slight exception for the Higgs boson, are all considered force carriers. Photons are the force carriers for the electromagnetic force. Gluons carry the strong force. W and Z bosons are the force carriers for the weak force. The Higgs boson is a bit different in that it is not necessarily a force carrier. Its existence is tied to the breaking of electroweak symmetry² and it gives fermions their mass.

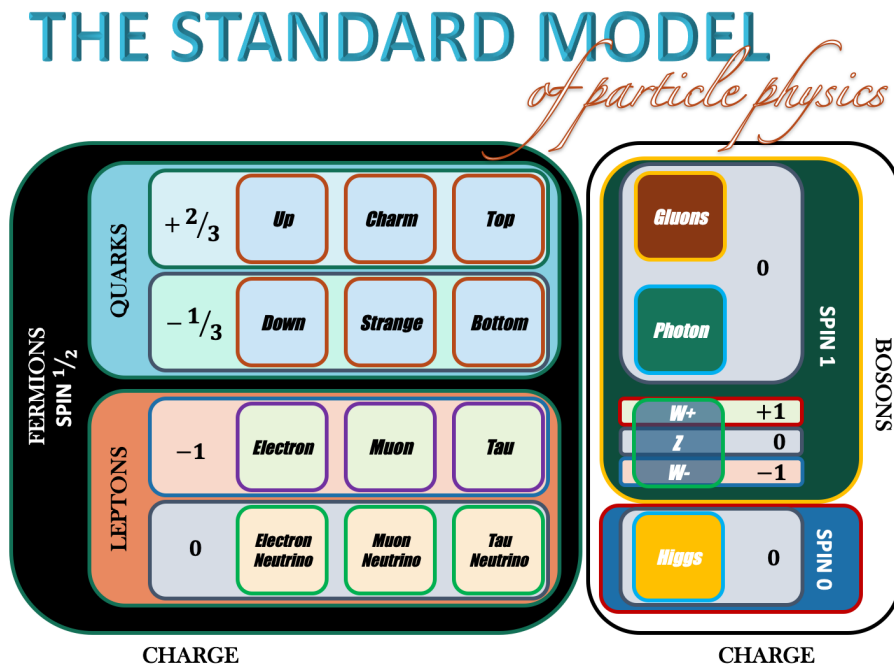


Fig. 1: The 17 fundamental particles of The Standard Model of Particle Physics.

The other subgroup is fermions, which are 12 particles³ that obey a Fermi-Dirac

¹The word "fundamental" here means that they are not made of constituent particles.

²In the early Universe, the electromagnetic and weak forces were one force. As the Universe began to cool, the symmetry that kept these two forces together broke. The Higgs boson essentially facilitated that breaking.

³Each of these fermions also have an associated anti-particle, which has the same mass but opposite electric charge. For example, an anti-electron (known as a positron) also has a mass of 511 keV/c² but a charge of +1.

statistical rule called the Pauli Exclusion Principle. Developed by Enrico Fermi, Paul Dirac and Wolfgang Pauli, this rule states that fermions cannot occupy the same place at the same time. Again in quantum physics language, no two fermions can be described by the same quantum numbers. There are two types of fermions in the Standard Model: 6 quarks and 6 leptons. Leptons, which include electrons, pions, tau and their associated neutrinos, cannot combine to make larger structures. Quarks, on the other hand, do combine to make larger structures, like protons, neutrons, atoms, molecules, people and light posts. They also obey the exclusion principle, which is why walking into a light post hurts. You both cannot be in the same place at the same time.

Quantum numbers, the things that help define the difference between fermions and boson, are conserved quantities that describe a quantum system. More precisely, quantum numbers are the eigenvalues of operators that commute with the Hamiltonian. These quantum numbers can describe quantities like angular momentum, spin or parity. The namesake to these numbers and this entire field of physics comes from the fact that many of these quantities often exist in steps of discrete quantities (*e.g.* integer or half-integer steps), thus quantized.

One of those quantized observables is something called spin. Because these fundamental particles are so incredibly small, they are considered featureless (or point-like). Therefore many of these quantum numbers have no physical meaning, they are simply mathematical constructs that tend to correspond to something physical we are familiar with. The spin quantum number is no exception. Fundamental fermions, as seen in Fig. 1, have spin 1/2, while fundamental bosons have integer spin of 0 or 1. Two, three or more quarks combine by way of gluons (*i.e.* the strong force). Two quarks combine to make particles called mesons⁴ (*e.g.* pions and kaons) and their spin states combine to form an overall integer 1, which also makes them bosons. Three quarks combine to make particles called baryons⁵ (*e.g.* protons and neutrons), which have spin 1/2 or 3/2 making them fermions as well. The collective group of quarks, mesons, and baryons are known as hadrons⁶.

Charge is another important quantized observable. When three quarks combine

⁴The word meson comes from the a Greek word $\mu\epsilon\sigma\omega\sigma$ ("mesos") meaning medium.

⁵Baryon comes from the a Greek word $\beta\alpha\rho\nu\sigma$ ("varys") meaning heavy.

⁶Comes from the Greek word $\alpha\delta\rho\omega\sigma$ ("adros") meaning massive or large. This one comes from the fact that point-like quarks can combine to make a particles much larger than the combined quarks themselves.

to make something like a proton or neutron, their charges also combine. A proton, for example, is made of two up quarks⁷ (each with charge $+2/3$) and a down quark (charge $-1/3$), so its overall charge is $+1$. A neutron is made of two down quarks and an up quark, so its charge is zero.

1.2 THE TROUBLE WITH UNDERSTANDING THE NUCLEON

Protons and neutrons make up the nucleus of an atom so they are called nucleons. These nucleons are not just made of three stationary quarks, but are very dynamic and busy particles. These three quarks that define whether it is a proton or neutron called valence quarks. However, there are also quark-antiquark pairs that are in a constant state of creation and annihilation, called sea quarks. Then there are gluons which are carriers of the strong force connecting quarks together. All of these particles have momenta and collectively define the structure of the nucleon. The trouble in physics has been defining this structure and the size of these nucleons as well as the momentum distribution of those fundamental particles that exist within it.

There has been a lot of effort exploring the structure and momentum distribution of the proton, yet there are some major puzzles that still exist. One of the most famous has to do with the proton spin called the “proton spin crisis”. This crisis refers to our collective inability to explain how all of the particles that exist in the proton conspire together to always give the proton spin $1/2$. Less famous puzzles include knowing the proton radius, where its mass comes from, and what the momentum distribution is of its fundamental constituent particles.

All of these puzzles also exist for the neutron, except with even less understanding. Whereas protons are easily confined to form targets for experiments, neutrons are not. Neutrons alone decay in about 15 minutes, and because they do not have electric charge, cannot be easily confined. One of experiments that set out to confirm or reject theories attempting to explain one of puzzles, the structure of the neutron and the momentum distribution of its constituents, is called the Barely Off-shell Nucleon Structure Experiment at 12 Giga-electron Volts (or BONuS12).

⁷Quark names are essentially meaningless. There is no physical characteristics that warrant a quark being called up or strange. They were simply given a name that stuck.

1.3 SCATTERING EXPERIMENTS AND BONUS12

In order to probe the enigmas of particles that are on the order of 50 trillion times smaller than a grain of sand, particle and nuclear physicists often use scattering experiments. These experiments accelerate particles to known energies and collide them on to a target. The collision of accelerated particles on a target causes them both to scatter and, in some cases, fragment. The scattered particles resulting from the collision then enter particle detectors where information like energy, position, momentum, and time are gathered by exploiting various physics processes. With this information physicists can extract things like the structure of nucleon or the momentum distribution of the fundamental constituents within it.

The Thomas Jefferson National Lab (JLab) in Newport News, Virginia contains a electron accelerator used for scattering experiments meant to explore nuclear and subatomic matter. Here is where, in 2005, the first BONuS Experiment ran in JLab's Experimental Hall B. The goal of that experiment was to explore the structure of the neutron and know more about the momentum distribution of the quarks and gluons inside. The results of the experiment made progress in narrowing error bars, which helped to begin confirming or denying some theories that exist attempting to describe these characteristics.

Jefferson Lab, in 2012, began an energy upgrade to bring the electron beam energy to 12 GeV, and with that came the development of an upgraded BONuS Experiment (called BONuS12). Just like the BONuS6 Experiment (that is the original BONuS Experiment which ran at 6 GeV), it is designed to explore the structure of the neutron and the momentum distribution of its fundamental constituent particles. Changes were made to improve the coverage of the detector, the momentum range that the RTPC can detect, and extend the fraction of quark momentum to neutron momentum range closer to one.

1.4 INCLUSIVE DEEP INELASTIC SCATTERING DATA ANALYSIS ON RUN GROUP A DATA

Throughout the rest of this work we will primarily discuss BONuS12, the physics necessary to understand its operation, and the efforts made to make the BONuS12 Experiment operational before it runs in Spring 2020. As a part of that comes the need to confirm that data coming in from Hall B experiments at JLab makes sense and is calibrated correctly.

While the BONuS12 RTPC will detect scattered protons, the scattered electron will enter the existing detectors in Hall B, so understanding that electron data is important. For that, a portion of this work will be dedicated to analyzing data from one of the first experiments that ran after the start of the 12 GeV physics era at JLab (*i.e.* Run Group A). The process known as inclusive deep inelastic scattering will be examined since we know much about it. In particular, we will look at what is known as the cross section of the process and compare it to simulations that use well known values of that cross section. This will hopefully provide evidence that the detectors within Experimental Hall B, where the BONuS12 Experiment will run, are working effectively and are calibrated correctly.

CHAPTER 2

PHYSICS FORMALISM

Talk about the development of current physics that describes nuclear and particle physics from the development of quantum physics to quantum electrodynamics and quantum chromodynamics.

2.1 NUCLEON STRUCTURE

The proton and neutron are the two components that make up a group called nucleons since they are the only two particles that make up the nucleus of an atom. They both interact through all four forces (*i.e.* strong nuclear, weak nuclear, electromagnetic, and gravitational). As mentioned in the Introduction, they are both fermions. Because they are both made up of three quarks, they are also both baryons.

The quarks that make up these nucleons (all baryons, in fact) and that are responsible for their quantum numbers are called *valence quarks*. The proton is made of two *up* valence quarks and one *down* valence quark, denoted by *uud*. The neutron is made up of two down valence quarks and an up valence quark, or *udd*. Of course, there are also *sea quarks* made of $q\bar{q}$ pairs, where $q\bar{q}$ is any variety of quark-antiquark pair. However, the strong interaction which binds all of these quarks together acts the same no matter the quark flavor¹. Therefore, the quark model does not predict any distinctions between protons and neutrons. In fact, from the view of the strong force, they are the identical particle in different states². Yet, protons and neutrons are clearly not identical particles.

There are obvious differences between two nucleons. One important difference between nucleons is their stability when not bound to each other. The proton is a stable particle on its own, with a lifetime of more than 2.1×10^{29} years. The neutron,

¹The word *flavor* is used to describe a type of quark. Remember there are 6 *flavors* of quarks: up, down, top, bottom, strange, and charm.

²There is a symmetry of the strong interaction in neutrons and protons called isospin (also referred to as isotopic or isobaric spin). Isospin is a dimensionless quantity that is not describe a physical "spin" of the particle. It does, however, offer a description of the two different states of nucleons. In particular, the projection of isospin along the z-axis (I_z or I_3) provides insight into the difference between protons and neutrons, which are otherwise almost identical particles. Protons have $I_z = 1/2$ and neutrons have $I_z = -1/2$.

however, has a lifetime of about 882 seconds (or about 15 minutes). The proton is the only nucleon that can exist in a nucleus on its own, such as in the hydrogen atom. Yet, the obvious difference in the two nucleons is their electric charge. The charge of the proton is +1 in units of electron charge, while the neutron is neutral (*i.e.* charge = 0). This charge arises from their valence quark content. The up quark has a charge equal to $q_u = +2/3$ and the down quark has a charge of $q_d = -1/3$, so for the proton with *uud* quarks

$$2q_u + q_d = 2(+2/3) + (-1/3) = +1 \quad (1)$$

and for the neutron with *ddu* quarks

$$2q_d + q_u = 2(-1/3) + (+2/3) = 0. \quad (2)$$

This charge distribution of quarks is well known for both nucleons. The momentum distribution of those quarks inside the nucleon is not as well known, especially for the neutron. The same is true for the overall structure of the nucleons, again more so for the neutron.

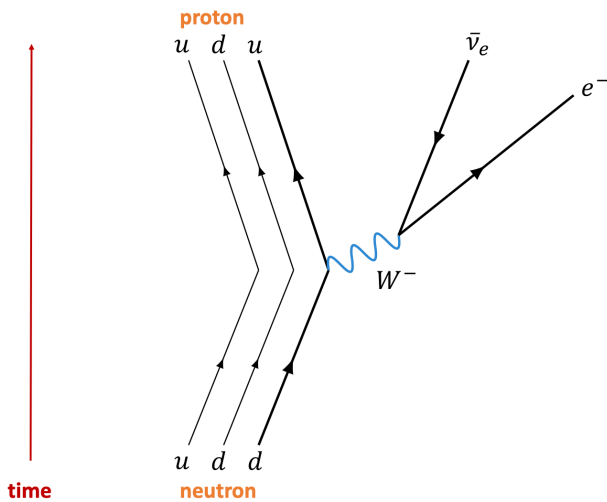
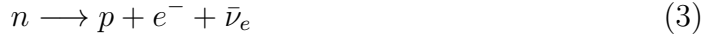


Fig. 2: The Feynman diagram of neutron decay.

The discrepancy of knowledge between the proton and the neutron is the last major difference of the nucleons we will discuss here, because it goes directly toward the principle of the BONuS12 Experiment. We know much more about the structure of the proton and momentum distribution of the quarks inside the proton for the

reason discussed in the last paragraph. That is, protons can exist outside of nuclei while neutrons soon decay via the weak interaction



seen in Fig. 2 as a Feynman diagram. Feynman diagrams were developed by physicist Richard Feynman to display particle interactions that occur in a relatively simplistic manner. Moving from the bottom to the top in the diagram of Fig. 2, we see a down quark within the neutron change states to an up quark mediated by the W^- boson emitting an electron (e^-) and electron antineutrino ($\bar{\nu}_e$). This decay happens within 15 minutes of a neutron being a free particle. That decay coupled with the fact that the neutron has no electric charge makes isolating neutrons to create a target for scattering experiments extremely difficult. Yet, scattering experiments are the primary means by which physicists study the structure of particles. Therefore, studying the structure of the neutron is inherently made difficult by this lack of free neutron target.

2.2 ELECTRON-SCATTERING KINEMATICS

To study the structure and physics of particles, nuclear and particle physicists use scattering experiments. There are two ways of creating a scattering experiment. One way is to accelerate a light particle (an electron, for example) and direct it toward a stationary target, which is the method used at Jefferson Lab in Newport News, Virginia. The other way is to accelerate two particles in opposite directions and then direct the two toward each other, which is the method used at the Large Hadron Collider (LHC) at CERN in Geneva, Switzerland. The physics or kinematics³ of both scattering experiments is essentially the same.

When the scattering particle and target collide, some of the momentum and energy of the scattering particle is transferred to that target particle. The way that nuclear and particle physicists express that energy and momentum is in something called its four-momentum. Classical momentum is a vector, which means it has a magnitude and direction. That direction is typically expressed in three dimensions

³The word kinematics refers to the mechanics of the particles without concern for the forces that caused the motion. Essentially, we are not concerned with *how* the particles were accelerated, just that they have a particular energy at the time of collision.

(for the familiar Cartesian coordinate system that would be along the x, y, and z-axis). Therefore a momentum can be expressed as $\mathbf{p} = (p_x, p_y, p_z)$, where \mathbf{p} is the momentum vector bold-faced to indicate that it is a vector. Because in particle physics, the particles travel close to the speed of light, we have to deal with special relativity. For the purposes of this work, special relativity essentially forces us to consider not just three-dimensional space, but four dimensional space-time with different reference frames for any non-accelerating moving objects. This drives us to require there be a four-dimensional space-time momentum $p = (p_0, p_1, p_2, p_3)$, where $p_1 = p_x$, $p_2 = p_y$, and $p_3 = p_z$ in Cartesian coordinates. The new term p_0 is equal to E/c , where E is the energy of the particle and c is the speed of light.

If we take this four-momentum

$$p_\mu = \left(\frac{E}{c}, p_x, p_y, p_z \right), \quad (4)$$

where μ is just an index indicating a particular particle and square it, we have

$$p^\mu p_\mu = -\frac{E^2}{c^2} + p_x^2 + p_y^2 + p_z^2 = -\frac{E^2}{c^2} + p^2. \quad (5)$$

This quantity should be invariant under a Lorentz transformation (meaning it remains the same no matter the non-accelerating reference frame) and is equal to the Lorentz scalar $-m^2 c^2$, which means

$$-\frac{E^2}{c^2} + p^2 = -m^2 c^2. \quad (6)$$

Multiplying both sides of Eq. 6 by $-c^2$ and rearranging a little gives us

$$E^2 = -p^2 c^2 + m^2 c^4, \quad (7)$$

which if we take the square root of both sides results in

$$E = \sqrt{(pc)^2 + (mc^2)^2}. \quad (8)$$

In the rest frame of the particle (*i.e.* the frame where the particle is considered to have no momentum, thus $p = 0$), this equation reduces to something that should be familiar. That is

$$E = mc^2. \quad (9)$$

This rough derivation provides a little insight to the power and purpose of using four-momentum. We will use this notation extensively throughout the rest of this work.

The other useful notation to understand is called natural units, where $c = \hbar = 1$. Under these units, Eq. 7 becomes

$$E^2 = p^2 + m^2. \quad (10)$$

While this offers much in the way of simplicity when working with complex equations, the disadvantage is that we lose information regarding dimensional analysis of the equation. Nevertheless, for the most part, we will use natural units in this work.

Now, consider an electron with four-momentum k scattering off of a nucleon with momentum p . The Feynman diagram for such an interaction is in Fig. 3, where k' and p' are the final momentum of the scattered electron and nucleon respectively. Here, q is the momentum of the virtual photon⁴ (typically denoted by γ^*) that mediates the interaction. That virtual photon momentum is defined as $q = k' - k$, which implies that it is the momentum lost by the scattered electron.

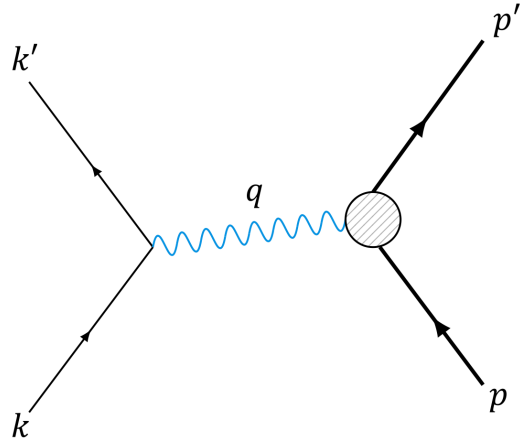


Fig. 3: Feynman diagram of an electron scattering from a proton.

There are some other important quantities to consider for electron scattering. The first is the square of that four-momentum transfer

$$q^2 = (k' - k)^2 = 2m_e^2 - 2(EE' - |\mathbf{p}||\mathbf{p}'| \cos \theta), \quad (11)$$

where m_e is the mass of the electron, E is the energy of the incident electron, E' is the energy of the scattered electron, $|\mathbf{p}|$ is the magnitude of the three-momentum of the

⁴The term "virtual" here may be misleading. It does not imply that the photon does not really exist. It refers to the short-lived exchange of the electromagnetic force.

incident nucleon, $|\mathbf{p}'|$ is the magnitude of the incident nucleon's three-momentum, and θ is the scattering angle of the electron. When we use the trigonometric identity $1 - \cos \theta = 2 \sin^2 \frac{\theta}{2}$ and take the electron mass to be zero, we get

$$q^2 \approx -4EE' \sin^2 \frac{\theta}{2}. \quad (12)$$

As a convention to make the quantity positive, we use $Q^2 = -q^2$, which will be used throughout the rest of this work. Another variable we need to analyze these electron scattering kinematics is the variable ν , which is the energy transfer of the electron to the nucleon via γ^* (*i.e.* the virtual photon) and is defined by

$$\nu = \frac{\mathbf{p} \cdot \mathbf{q}}{M}. \quad (13)$$

Here, p is the four-momentum of the incident nucleon, q is the four-momentum of the incident electron and M is the nucleon mass. In the laboratory frame, the nucleon is at rest (*i.e.* $p = (M, \mathbf{0})$)⁵, and $q = (E - E', \mathbf{q})$, so the energy transferred by the virtual photon to the nucleon in the laboratory frame would be

$$\nu = E - E'. \quad (14)$$

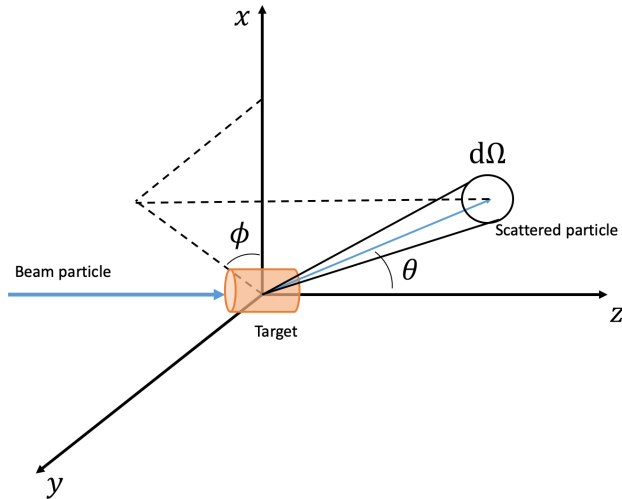


Fig. 4: Scattering process on a quasi-static Differential cross section.

Whenever we deal with collisions of particles, there is a probability associated with the reaction between that projectile and target depicted in Fig. 4. That probability

⁵Just like other three-dimensional vectors, when bolded, $\mathbf{0}$ represents $(0,0,0)$.

is called the *cross section* and with it often comes a wealth of knowledge about the dynamics of the interaction itself. In many reactions we deal with what is known as the *differential cross section*, which offers a more realistic insight to only a fraction of reactions. This differential cross section is ratio of the number of particles per unit time scattered into a bit of the solid angle $d\Omega$. Mathematically, the cross section of a spinless particle scattered from a static point charge the differential cross section can be written as

$$\frac{d\sigma}{d\Omega} = \frac{\alpha^2}{4E^2 \sin^4 \frac{\theta}{2}}, \quad (15)$$

where α is known as the fine-structure constant equal to $e^2/4\pi \approx 1/137$, E is the energy of the incident electron, and θ is the scattering angle of the electron in the laboratory frame. Eq. 15 is known as the Rutherford Formula and is the simplest theoretical scattering case. If we include the electron spin, we get

$$\frac{d\sigma}{d\Omega} = \frac{\alpha^2 \cos^2 \frac{\theta}{2}}{4E^2 \sin^4 \frac{\theta}{2}}, \quad (16)$$

which is known at the *Mott cross section* (we will from now on denote this particular cross section by $(\frac{d\sigma}{d\Omega})_{\text{Mott}}$). If we next introduce the mass of the point-like target M , that target particle will recoil, and so we get a scattered electron energy of

$$E' = \frac{E}{1 + \frac{2E}{M} \sin^2 \frac{\theta}{2}}, \quad (17)$$

modifying the Mott cross section to

$$\frac{d\sigma}{d\Omega} = \left(\frac{d\sigma}{d\Omega} \right)_{\text{Mott}} \cdot \frac{E'}{E} \left[1 - \frac{q^2}{2M^2} \tan^2 \frac{\theta}{2} \right] = \frac{\alpha^2 \cos^2 \frac{\theta}{2}}{4E^2 \sin^4 \frac{\theta}{2}} \cdot \frac{E'}{E} \left[1 - \frac{q^2}{2M^2} \tan^2 \frac{\theta}{2} \right]. \quad (18)$$

As that target mass M increases, this equation reduces to the Mott cross section.

We are beginning to approach a more realistic mathematical description of scattering, so we must discuss the various types that exist. In Fig. 3 if both particles remain intact after the collision, it is called *elastic scattering*. Like pool balls, they essentially bounce off each other, of course through the exchange of that virtual photon. When the amount of energy transfer increases (*i.e.* when q increases), different types of scattering arise. We need to understand these types of scattering in more depth to understand the BONuS12 Experiment.

2.3 ELASTIC SCATTERING

When the momentum transfer, or more specifically Q^2 , is low, there is a higher probability that the lepton (at JLab, that lepton is an electron) essentially bounces off of the target particle (typically a nucleon) in what is known as elastic scattering. Whatever momentum is transferred does not force the nucleon into excited states (called resonances) or break it apart entirely (deep inelastic scattering). In a situation like Fig. 3 when scattering elastically

$$k + p \longrightarrow k' + p' \quad (19)$$

or

$$k + p = k' + p' \quad (20)$$

indicating the conservation of energy and momentum. Here k and p are the incident electron and nucleon four-momenta respectively, and k' and p' are the scattered electron and nucleon respectively. In this elastic case,

$$(k + q)^2 = p^2 = M_N^2, \quad (21)$$

where M_N is the mass of the nucleon.

Because these particles are not point-like, we cannot simply use the Mott Equation (Eq. 16) to calculate the cross section of this elastic-scattering process. If we scatter electrons from some particle with a charge distribution $\rho(r)$ (here $\rho(r)$ is the charge distribution which is dependent on the distance away r from the charge source), like a proton, the scattering amplitude is modified by something called a form factor

$$F(q^2) = \int d^3r e^{i\mathbf{q}\cdot\mathbf{r}} \rho(r). \quad (22)$$

This particular form factor in Eq. 22 is an integral over volume of that charge distribution times the plane-wave of the particle, and is just the Fourier Transform of the charge density. As the name suggests this form factor provides insight into the composite structure of that particle. When this form factor is squared, it serves as a multiplier to the the Mott cross section, giving us an expression for elastic scattering

$$\frac{d\sigma}{d\Omega} = \left(\frac{d\sigma}{d\Omega} \right)_{\text{Mott}} [F(q^2)]^2, \quad (23)$$

where the Mott cross section found in Eq. 16 is elastic electron scattering off a point-like Dirac particle⁶. This gives us a useful description of elastic electron-proton scattering.

The last thing to do regarding the elastic scattering cross section is to expand the expression into the kinematic variables we can measure. We accomplish this by defining a scattering probability amplitude \mathcal{M} such that in the lab frame

$$\frac{d\sigma}{d\Omega} = \frac{1}{64\pi^2} \left(\frac{1}{M_p + 2E \sin^2 \frac{\theta}{2}} \right)^2 |\mathcal{M}_{fi}|^2, \quad (24)$$

where we neglect the small electron mass, M_p is the mass of the proton, E is the incident electron energy, and θ is the scattering angle of the electron in the lab frame. The term $|\mathcal{M}_{fi}|^2$ is shorthand for

$$|\mathcal{M}_{fi}|^2 = |\langle f | \mathcal{M} | i \rangle|^2, \quad (25)$$

which means that we find the modulus squared expectation value of the observable \mathcal{M} for the initial and final states. If the polarizations are not observed, this must be averaged over initial spin states of the modulus squared of the scattering amplitudes and the summed over the final spin states of $|\mathcal{M}|^2$. Mathematically, using s and S for initial spin states of the electron and proton respectively and s' and S' for final spin states, it can be expressed as

$$|\mathcal{M}_{fi}|^2 = \frac{1}{2} \sum_{s,S} \sum_{s',S'} |\mathcal{M}|^2, \quad (26)$$

where \mathcal{M} is the scattering probability amplitude.

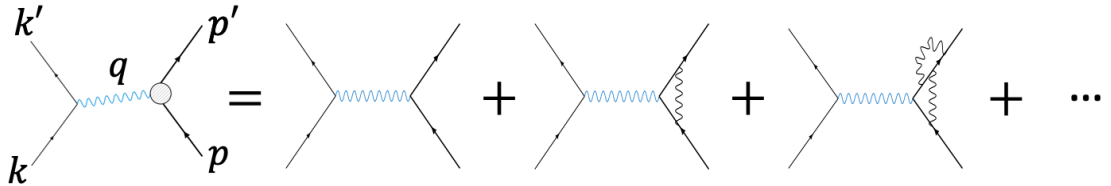


Fig. 5: The contributions of higher order diagrams.

The scattering probability amplitude cannot be known exactly because of the processes beyond the first order (tree level) that could occur in Fig. 3 at the proton- γ^* vertex blob (these contributions can be seen in Fig. 5). However, we can handle the

⁶A Dirac particle refers to a particle whose wave-function ψ obeys the Dirac equation $(i\cancel{\partial} - m)\psi = 0$. The “slashed” notation is used to indicate $\cancel{\partial} \stackrel{\text{def}}{=} \gamma^\mu \partial_\mu$, where γ^μ are the set of Pauli matrices.

mathematical description of these processes by expressing the scattering probability amplitude matrix it in terms of the leptonic and hadronic tensors, we have

$$|\mathcal{M}|^2 = \frac{e^4}{Q^4} \ell_{\mu\nu} W^{\mu\nu}. \quad (27)$$

The leptonic tensor $\ell_{\mu\nu}$ is associated with the coupling of the virtual photon to the electron (more generally the coupling of the exchange boson to the lepton), and for unpolarized scattering can be expressed as

$$\ell_{\mu\nu} = \bar{u}(k', s') \gamma^\mu u(k, s) \bar{u}(k, s) \gamma^\nu u(k', s'). \quad (28)$$

The term $u(k)$ is the Dirac spinor. For the electron (a spin-1/2 fermion), there are two spin states (*i.e.* up or down) so there are two associated spinors that could exist here

$$u_\uparrow(k) = \begin{pmatrix} 1 \\ 0 \\ \frac{k_z}{E+m} \\ \frac{k_x+ik_y}{E+m} \end{pmatrix} \text{ and } u_\downarrow(k) = \begin{pmatrix} 0 \\ 1 \\ \frac{k_x-ik_y}{E+m} \\ \frac{-k_z}{E+m} \end{pmatrix}. \quad (29)$$

In Eq. 28, γ^μ are the gamma matrices. When summed and averaged over spins, the leptonic tensor becomes

$$\begin{aligned} \ell_{\mu\nu} &= \text{Tr} \left[\frac{\not{k}' + m}{2m} \gamma^\mu \frac{\not{k} + m}{2m} \gamma^\nu \right] \\ &= \frac{1}{m^2} \text{Tr}(\not{k}' \gamma^\mu \not{k} \gamma^\nu + m^2 \gamma^\mu \gamma^\nu) \\ &= 2(k'^\mu k^\nu + k^\mu k'^\nu - g^{\mu\nu} k' \cdot k). \end{aligned} \quad (30)$$

Thus far we have from Eq. 27

$$|\mathcal{M}|^2 = \frac{e^4}{Q^4} 2(k'^\mu k^\nu + k^\mu k'^\nu - g^{\mu\nu} k' \cdot k) W^{\mu\nu}, \quad (31)$$

where $g^{\mu\nu}$ is the metric tensor.

We must now take a look at the hadronic tensor $W^{\mu\nu}$, which is more complicated because we must take into account for the proton's structure. In fact, the hadronic tensor cannot be known exactly. It can, however, be expanded to the second order as

$$W^{\mu\nu} = \langle p | J^\nu | p' \rangle \langle p' | J^\mu | p \rangle, \quad (32)$$

which depends on the J^μ current matrix elements. That current between two nucleon states

$$\langle p | J^\mu(0) | p' \rangle = \bar{U}(p') \left[F_1(Q^2) \gamma^\mu + F_2(Q^2) \frac{i\sigma^{\mu\nu}}{2M_N} \right] U(p) \quad (33)$$

gives rise to two form factors, $F_1(Q^2)$ which is called the Dirac form factor and $F_2(Q^2)$ called the Pauli form factor. Here $\sigma^{\mu\nu} = \frac{i}{2}[\gamma^\mu, \gamma^\nu]$ and we denote the difference between the lower-case $u(k, s)$ electron spinors from Eq. 28 and upper-case $U(p)$ nucleon spinors. If we introduce the more physically interesting Sach's electric and magnetic form factors respectively

$$G_E(Q^2) = F_1(Q^2) + \frac{Q^2}{4M_N^2}F_2(Q^2)$$

$$G_M(Q^2) = F_1(Q^2) + F_2(Q^2),$$

then the hadronic tensor can be written as

$$\begin{aligned} W^{\mu\nu} &= 2(p'^\mu p^\nu + p'^\nu p^\mu - g^{\mu\nu}(pp' - M_N^2))G_M^2 \\ &\quad - 2F_2 G_M (p + p')^\mu (p + p')^\nu + F_2^2 \frac{M_N^2 + p \cdot p'}{2M_N^2} (p + p')^\mu (p + p')^\nu \\ &= (-q^\mu q^\nu + g^{\mu\nu}q^2)G_M^2 + (p + p')^\mu (p + p')^\nu \frac{G_E^2 + \tau G_M^2}{1 + \tau} \\ &= g^{\mu\nu}q^2 G_M^2 + 4p^\mu p^\nu \frac{G_E^2 + \tau G_M^2}{1 + \tau} + \dots, \end{aligned} \tag{34}$$

where we define $\tau = Q^2/4M_N^2$ to simplify the expression. Because of current conservation, the terms contain factors of q^μ are omitted with the ellipses, since they do not contribute to the cross section.

Substituting our expressions for the leptonic and hadronic tensors for elastic scattering in the lab frame and contracting them, we arrive at

$$\frac{d\sigma}{d\Omega} = \left(\frac{d\sigma}{d\Omega} \right)_{\text{Mott}} f_{\text{rec}} \left[\frac{G_E^2(Q^2) + \tau G_M^2(Q^2)}{1 + \tau} + 2\tau G_M^2 \tan \frac{\theta}{2} \right], \tag{35}$$

where $\left(\frac{d\sigma}{d\Omega} \right)_{\text{Mott}}$ comes from Eq.16 (*i.e.* the Mott cross section) and f_{rec} is the recoil factor equal here to E'/E . As Q^2 gets very high, τ increases and magnetic form factor $G_M(Q^2)$ dominates. This gives a more physical description of the elastic scattering cross section in terms of kinematic variables that can be measured through scattering experiments.

One more kinematic variable that needs to be introduced offers insight into cases when scattering enters into inelastic regimes. The invariant mass squared W^2 (not to be confused with the hadronic tensor $W^{\mu\nu}$) of the photon-nucleon system, is defined mathematically as

$$W^2 = (q + p)^2 = M_N^2 + 2M_N\nu - Q^2, \tag{36}$$

where $\nu = E - E'$ is the energy transferred from the electron to the nucleon via virtual photon (γ^*). In the elastic scattering case, $W^2 = M_N^2$, because Q^2 and thus ν tend to be small (*i.e.* $E \ll M_N$). As Q^2 increases, instead of simply bouncing off of the nucleon, the energy transferred to the nucleon begins changing the state of the quarks within the nucleon.

2.4 RESONANCE REGION

Changing the state of a quark within the nucleon results in excited states of that nucleon, called *resonances*. The region where resonances occur is $M_N^2 < W^2 < 4 \text{ GeV}^2$, and is called the *resonance region*. There are 6 families of resonances that depend on the characteristics of the resonant particles. Particles containing only u and d quarks whose isospin $I = \frac{1}{2}$ are denoted by N . The Δ family of resonances also have only u and d quarks, but have $\frac{3}{2}$ isospin. When $I = 0$ and the particle contains u , d and one c , s , or b quark, it is called a Λ resonance. The Σ resonance also has u , d plus one c , s , or b quark, but with $I = 1$. When only one u or d quark exists with two c , s , or b quarks with $I = \frac{1}{2}$, it is a Ξ resonance. Finally, when $I = 0$ and only c , s , or b quarks are present, it is known as an Ω resonance.

Unlike the ground state of nucleons, these excited states are extremely short lived (on the order of 10^{-23} seconds). After their short life, these resonances decay into more stable hadrons. Detection of these hadrons is what provides proof of the existence of resonant states. For example, a common resonance $\Delta^0(1232)$, which is the lowest lying resonance with a mass of 1.232 GeV, predominately decays via the strong interaction into a pion (π^0) and a neutron (n). The entire interaction begins at the first step of creating an excited state



then decays into



However, because these resonances are so short-lived, it is convention to express the entire interaction as



One reason for this convention is that there are many resonances that can produce the same end particles (*i.e.* π^0 and n in our example). Knowing exactly what resonance

produced those end particles can be difficult. In the example of Eq. 39, the Δ^0 has the same quark makeup as the neutron (*i.e.* udd), but is much heavier. Measuring the invariant mass of the resulting particles is one of the few ways to understand what resonance occurred.

Similar to elastic scattering, interactions with resonances can be described using form factors. The analogous cross section is

$$\frac{d\sigma}{d\Omega} = \left(\frac{d\sigma}{d\Omega} \right)_{\text{Mott}} f_{\text{rec}} \left(\frac{|G_E|^2 + \tau^*|G_T|^2}{1 + \tau^*} + 2\tau^*|G_T|^2 \tan^2 \frac{\theta}{2} \right) R(W), \quad (40)$$

where f_{rec} is the recoil factor of the proton, τ^* is the analogous kinematic quantity of τ from elastic scattering, G_E and G_T are the resonance longitudinal and transverse form-factors respectively, and $R(W)$ is called the resonance line shape. In inelastic scattering of resonances

$$f_{\text{rec}} = \frac{E'}{E} \left[\frac{1}{1 - \frac{(W_R^2 - M_N^2)}{2M_N E}} \right], \quad (41)$$

$$\tau^*|G_T|^2 = \frac{1}{2}(|G_+|^2 + |G_-|^2), \quad (42)$$

and

$$R(W) = \frac{2\pi^{-1}W_R M_N \Gamma_R}{(W^2 - W_R^2)^2 + W_R^2 \Gamma_R^2}. \quad (43)$$

The quantities W_R and Γ_R refer to the resonance mass and width respectively. If the resonance width is small enough (*i.e.* when $W_R = M_N$ and $W_R \Gamma_R \rightarrow 0$), $R(W)$ becomes a δ -function and the resonance cross section reduces to that of an elastic cross section.

At low Q^2 , we can describe interactions by constituent quarks models. At high Q^2 we enter a region best described with perturbative quantum chromodynamics (pQCD). We will discuss more about pQCD in a later section. The resonant region is an important bridge between these two regimes. Determining resonance form factors allows us to describe the resonance transition the same way elastic form factors describes elastic interactions.

2.5 DEEP INELASTIC SCATTERING

Once the energy transferred to the nucleon (Q^2) becomes large enough, the probability of creating excited (resonance) states decreases and there becomes a higher

probability of the virtual photon “elastically” scattering off a quark inside the nucleon. This is known as *deep* inelastic scattering. This happens around when $W > 2$ MeV and $Q^2 > 1$ GeV 2 in an area known as the *continuum*. In this regime we can probe the inner structure of the nucleon.

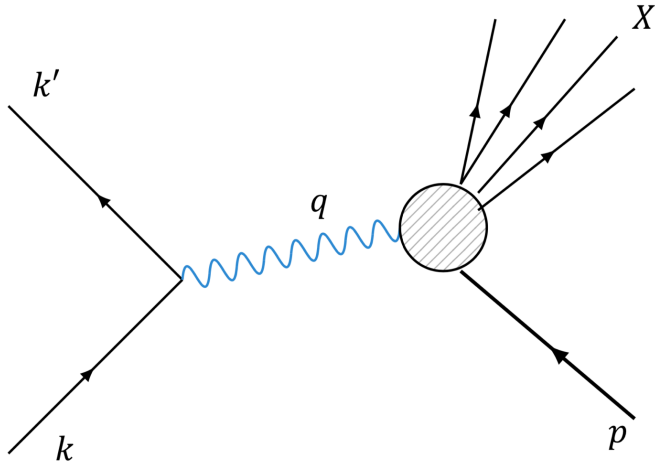


Fig. 6: Feynman diagram of an inelastic electron scattering from a proton.

However, because the energy transfer is so high, the proton often breaks apart in the interaction

$$ep \longrightarrow eX, \quad (44)$$

where X denotes all possible particles that might emerge from the proton-electron collision. The Feynman diagram also must be altered from Fig. 3 to Fig. 6, where X again represents all possible emerging particles. The other change from elastic and inelastic resonance-region scattering is to the cross section. This deep-inelastic scattering cross section can be written as

$$\frac{d\sigma}{dE'\Omega} = \frac{4\alpha^2 E'^2}{q^4} W_2(\nu, Q^2) \cos^2 \frac{\theta}{2} + 2W_1(\nu, Q^2) \sin^2 \frac{\theta}{2}, \quad (45)$$

where W_1 and W_2 are called inelastic structure functions. These structure functions are the analogs to the form factors in Eq. 35 for elastic scattering. There is much more to discuss about deep-inelastic scattering, but first we must discuss how to treat scattering off of quarks (or more broadly, partons) within a nucleon with an approach called *scaling*.

2.6 PARTONS AND BJORKEN-SCALING

The way we probe inside nucleons is with the exchange of small wavelength (large Q^2) virtual photons, which break apart the proton. This can be handled using the inelastic structure functions W_1 and W_2 , which are functions of the energy lost by the electron due to proton recoil (*i.e.* ν) and the negative four-momentum squared of the virtual photon (*i.e.* Q^2). When the virtual photon has a small enough wavelength (large enough Q^2), the nucleon that was once described by Eq. 35 starts to look more like a free Dirac particle described by

$$\frac{d\sigma}{dE'd\Omega} = \frac{4\alpha^2 e_q^2 E'^2}{q^4} \left(\cos^2 \frac{\theta}{2} - \frac{q^2}{2m^2} \sin^2 \frac{\theta}{2} \right) \delta \left(\nu + \frac{q^2}{2m} \right). \quad (46)$$

Remarkably, this is the equation for an electron elastic scattering from a structureless particle. Here e_q is the fractional charge of that structureless particle and m is that particle's mass. This particle inside the nucleon was eventually called a quark.

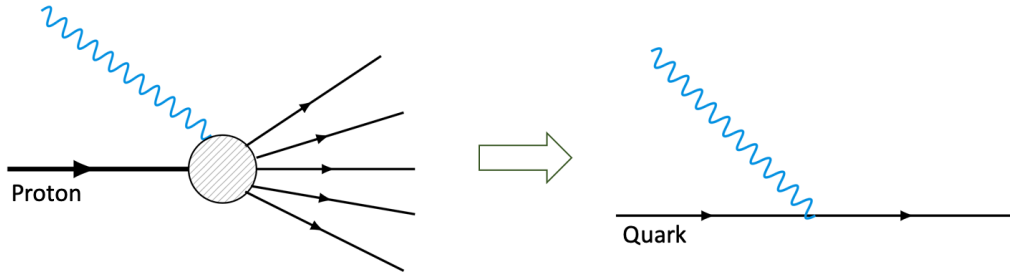


Fig. 7: The transition from inelastic scattering to deep inelastic scattering of a virtual photon and the quark within a nucleon.

In this case, where the photon elastically scatters off of a quark within the nucleon described by Eq. 46, the nucleon structure functions become

$$2W_1^{\text{point}} = \frac{Q^2}{2m^2} \delta \left(\nu - \frac{Q^2}{2m} \right) \quad (47)$$

and

$$W_2^{\text{point}} = \delta \left(\nu - \frac{Q^2}{2m} \right). \quad (48)$$

Here and thus in Eq. 46 there exists the delta function that conserves energy in the interaction. Fig. 7 shows the resulting diagram when we take the right side of Fig. 6 (the left side of Fig. 7) and begin to probe a single quark inside the nucleon (the right side of Fig. 7). This reduction is representative of the electron elastically scattering off a quark in the nucleon.

If we take Eq. 47 and 48, using the identity $\delta(x/a) = a\delta(x)$, we can write

$$2mW_1^{\text{point}}(\nu, Q^2) = \frac{Q^2}{2m\nu} \delta\left(1 - \frac{Q^2}{2m\nu}\right)$$

$$\nu W_2^{\text{point}}(\nu, Q^2) = \delta\left(1 - \frac{Q^2}{2m\nu}\right). \quad (49)$$

These equations for the structure functions are now dimensionless and depend on only the ratio $Q^2/2m\nu$, which is both important and useful. That usefulness is as follows: when Q^2 is high enough, the virtual photon begins to elastically scatter off of structureless (point) particles within the nucleon and can be described using the dimensionless structure functions

$$MW_1(\nu, Q^2) \xrightarrow[\text{large } Q^2]{} F_1(x_B)$$

$$\nu W_2(\nu, Q^2) \xrightarrow[\text{large } Q^2]{} F_2(x_B). \quad (50)$$

Here x_B is introduced as the Bjorken- x scaling variable defined as

$$x_B = \frac{Q^2}{2M\nu}, \quad (51)$$

which describes the momentum fraction of a quark or gluon within a nucleon. Up to this point, we have only been discussing interactions between the virtual photon and the quarks within the nucleon, but that virtual photon can also interact with gluons that exists in the nucleon. Collectively, these quarks and gluons in the nucleon are known as partons. The Bjorken- x scaling variable can describe the momentum fraction of any parton within a nucleon.

The relationship between the structure functions $F_1(x_B)$ and $F_2(x_B)$ is

$$2x_B F_1(x_B) = F_2(x_B) = \sum_i e_i^2 f_i(x_B), \quad (52)$$

where in the right side of this expression we have a sum over partons (the parton index is i) of the square of that parton's charge squared (e_i^2) times $f_i(x_B)$ known at the parton distribution function. The parton distribution function (or PDF)

$$f_i(x_B) = \frac{dP_i}{dx_B} \quad (53)$$

describes the probability P_i that a struck parton i carries a fraction (x_B) of the nucleon's momentum.

Because $F_1(x_B)$ can be calculated using $F_2(x_B)$ using the Callan-Gross relation $2x_B F_1(x_B) = F_2(x_B)$, the F_2 structure function is the more important term here to examine experimentally and is of interest in the BONuS12 Experiment. For deep-inelastic electron-proton scattering, the $F_2^p(x_B)$ structure function is

$$\frac{1}{x_B} F_2^p(x_B) = \left(\frac{2}{3}\right)^2 [u^p(x_B) + \bar{u}^p(x_B)] + \left(\frac{1}{3}\right)^2 [d^p(x_B) + \bar{d}^p(x_B)] \quad (54)$$

$$+ \left(\frac{1}{3}\right)^2 [s^p(x_B) + \bar{s}^p(x_B)], \quad (55)$$

where p superscript denotes that we are dealing with the proton structure, and the PDF $f_i(x_B)$ is replaced with the first letter of the quark name (*e.g.* the up quark and antiquark PDF's are denoted as $u^p(x_B)$ and $\bar{u}^p(x_B)$ respectively). The contributions of quarks heavier than the strange quark have been assumed to be negligible here. The neutron structure function $F - 2^n(x)$, where we have dropped the B in x_B , is

$$\frac{1}{x} F_2^n(x) = \left(\frac{2}{3}\right)^2 [u^n(x) + \bar{u}^n(x)] + \left(\frac{1}{3}\right)^2 [d^n(x) + \bar{d}^n(x)] \quad (56)$$

$$+ \left(\frac{1}{3}\right)^2 [s^n(x) + \bar{s}^n(x)]. \quad (57)$$

This looks similar to the F_2^p structure function because the proton and neutron are together part of an isospin doublet. When particles are members of an isospin doublet, they can transform into each other under an $SU(2)$ transformation

$$\binom{p}{n} \xrightarrow{SU(2)} \exp\left(-\frac{i}{2}\theta_a \sigma_a\right) \binom{p}{n},$$

where p and n are proton and neutron states, and σ_a are the Pauli matrices. This transformation means that the quark contents of the proton and neutron are related.

2.7 NUCLEON STRUCTURE-FUNCTION RATIO F_N^2/F_P^2

We can exploit this relation between quark contents of protons and neutrons to study the structure of nucleons, in particular the neutron structure. That relationship between quark contents means

$$\begin{aligned} u^p(x) &= d^n(x) \equiv u(x), \\ d^p(x) &= u^n(x) \equiv d(x), \end{aligned} \quad (58)$$

$$s^p(x) = s^n(x) \equiv s(x). \quad (59)$$

Each nucleon consists not only of u_v and d_v quarks that determine the quantum numbers of the nucleon (called *valence* quarks, hence the subscript v), but many quark-antiquark pairs in a constant state of creation and annihilation (known as *sea* quarks). In the first order approximation, we can assume that the lighter quark-antiquark pairs $u_s\bar{u}_s$, $d_s\bar{d}_s$, and $s_s\bar{s}_s$ contribute to this "sea" and we can neglect contributions from the heavier quark-antiquark pairs $c_s\bar{c}_s$ and so on.

This approximation of the nucleon structure results in adding the sea quarks to the contributions of each quark type. That is

$$u(x) = u_v(x) + u_s(x), \quad (60)$$

$$d(x) = d_v(x) + u_s(x), \quad (60)$$

$$u_s(x) = \bar{u}_s(x) = d_s(x) = \bar{d}_s(x) = s_s(x) = \bar{s}_s(x) = S(x), \quad (61)$$

where we now use $S(x)$ for all sea quark contributions. If we combine this relationship with our expressions for the proton and neutron structure functions Eq. 54 and Eq. 56 respectively, we get

$$\frac{1}{x}F_2^p = \frac{1}{9}[4u_v + d_v] + \frac{4}{3}S \quad (62)$$

and

$$\frac{1}{x}F_2^n = \frac{1}{9}[u_v + 4d_v] + \frac{4}{3}S, \quad (63)$$

where the $\frac{4}{3}$ comes from summing over all six sea quark distributions. In the low x limit, ADD PLOT OF QUARK CONTENT AS F'N OF X

2.8 DIFFICULTIES IN EXTRACTING F_N^2/F_P^2 FROM DEUTERIUM

2.8.1 BOUND NUCLEON STRUCTURE

2.8.2 BACKGROUNDS

2.9 BARELY OFF-SHELL NUCLEON STRUCTURE

CHAPTER 3

THE BONUS12 EXPERIMENT

The BONuS12 Experiment will be conducted at the Thomas Jefferson National Laboratory (JLab) in Newport News, Virginia. JLab was founded in 1984 with the intent of studying the structure of nuclear matter. The unique accelerator that was built at JLab, called the Continuous Electron Beam Accelerator Facility (CEBAF), allowed for the realization of that intent by providing the ability to probe atomic nuclei at the quark level. In order to understand the BONuS12 Experiment, we must first understand CEBAF and the Hall B spectrometer that the BONuS12 RTPC will be installed in. Then we will discuss the RTPC design, components, and construction.

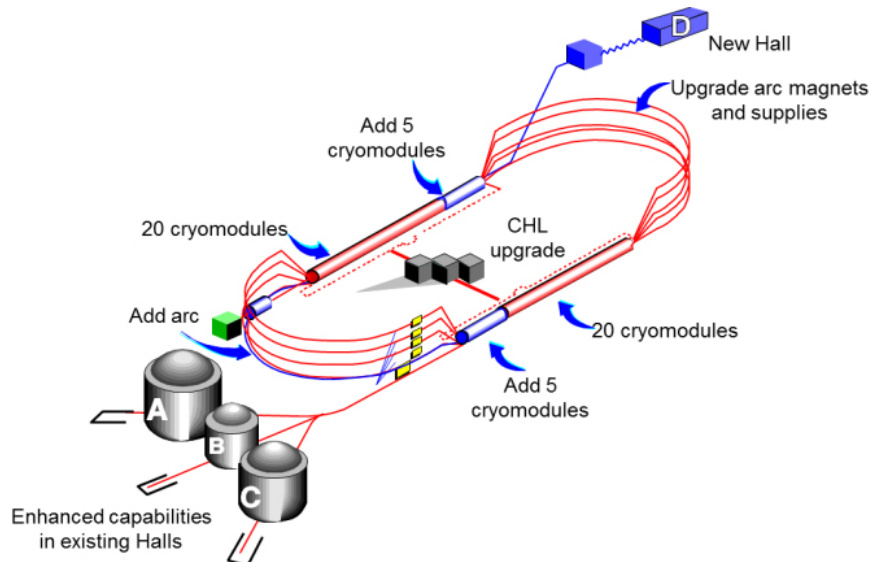


Fig. 8: CEBAF upgraded for the 12 GeV era.

3.1 CONTINUOUS ELECTRON BEAM ACCELERATOR FACILITY

The construction of the Continuous Electron Beam Accelerator Facility (CEBAF) was completed in 1994. It originally consisted of two antiparallel linear accelerators (LINACs) connected by nine recirculation arcs that accelerated electrons to an energy of 6 GeV at a current of up to 300 μ A. In 2004, JLab began an energy upgrade

that would allow CEBAF to supply electrons up to 12 GeV. The same framework used for the 6 GeV accelerator would be used for the 12 GeV era. That is, each pass around the accelerator would increase the energies, which was 1-1.2 GeV/pass during the 6 GeV era [1] and 2.2 GeV/pass after the 12 GeV upgrade. Originally, that meant 5 passes would produce 6 GeV electrons before they were fed into the three existing experimental halls (*i.e.* Hall A, Hall B, and Hall C). In addition to the energy upgrade that increases the energy, a new experimental hall was built (*i.e.* Hall D). That leads to 5 passes creating around 10.5 GeV electron beam to Halls A, B and C. Hall D received electrons from 5.5 passes around the accelerator creating the 12 GeV electron beam energy. As Fig. 8 shows, the upgrade consisted of addition 5 additional cryomodules, an additional recirculation arc, increased capacity of the Central Helium Liquefier (CHL), and improvements in the curving magnet.

The electrons are accelerated in CEBAF by way of the LINACs. These LINACs contain a set of superconducting Niobium accelerating cavities with a magnetic field that oscillates at a frequency of 1.5 GHz. Electrons are injected in bunches into the accelerator with an energy of 45 MeV at the same frequency as the cavities every 0.7 ns. These electrons then circulate around, increasing in energy each pass by the LINACs. Once the desired energy for a given hall is reached, every 2.1 ns magnetic fields inside the arcs force the electrons into specific central trajectories that guides them into that hall. The beam is considered "continuous" because of the high operating frequency at which CEBAF can operate up to its maximum capacity at 200 μ A.

3.2 CEBAF LARGE ACCEPTANCE SPECTROMETER

Once the electrons are accelerated to a desired energy, they are received by the halls, where they enter each hall's spectrometer. A spectrometer is just an instrument (or collection of instruments) that measure and analyze a range (or spectrum) of processes or reactions. Because BONuS12 will operate in Hall B, here we will focus on the components and operation of Hall B's spectrometer, called the CEBAF Large Acceptance Spectrometer at 12 GeV (or CLAS12). As the name suggests, CLAS12 is an evolution of CLAS6 (or just CLAS as it was known before talk of the energy upgrade), which was the original spectrometer built for Hall B.

CLAS12 (see Fig. 9) consists of two major groups of detectors, which together allow for detection and identification of particles over a large scattering angle, thus

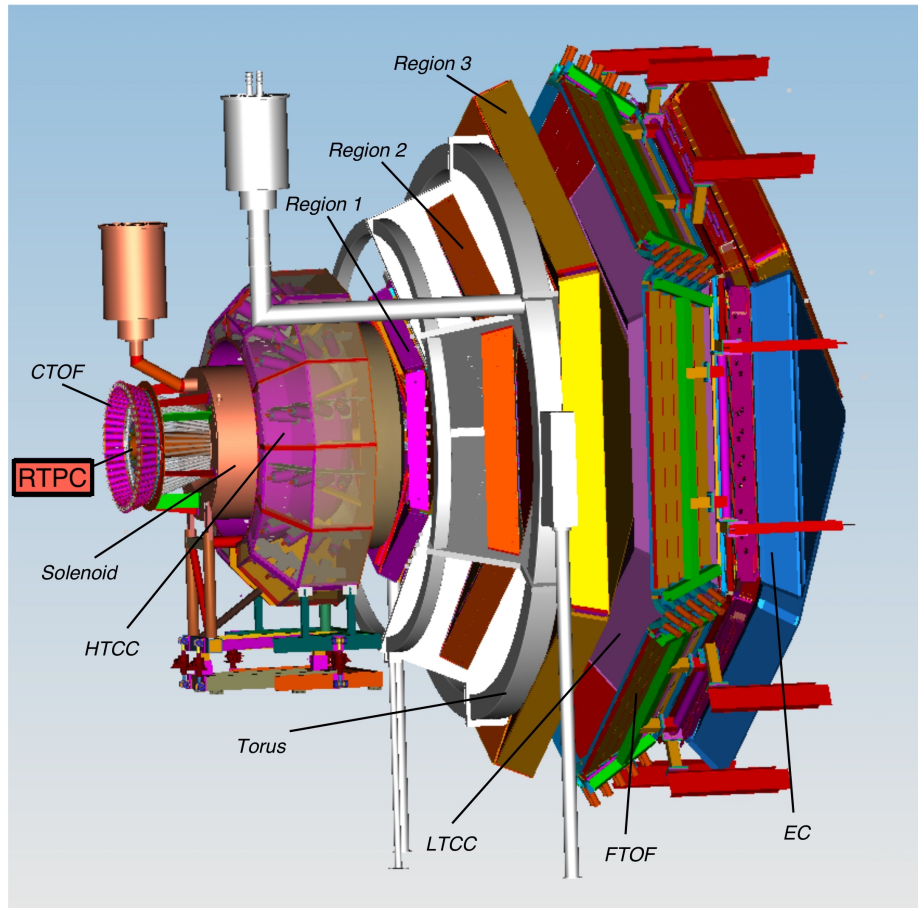


Fig. 9: The CEBAF Large Acceptance Spectrometer at 12 GeV (CLAS12).

the “Large Acceptance” in the name CLAS12. The Forward Detector (FD) covers scattering angles of between 5-40 degrees, and consists of a torus magnet, Cherenkov counters, a time of flight detector, drift chambers and electromagnetic calorimeter. The other group of detectors is known as the Central Detector (CD), and covers scattering angles between 40-125 degrees. The CD consists of a solenoid magnet, time of flight detector and finally, the BONuS12 RTPC. We will discuss each of these detectors, with a bit more focus on the RTPC.

3.2.1 TORUS MAGNET

The torus magnet is comprised of six superconducting coils arranged symmetrically around the beamline to create a azimuthally-symmetric magnetic field up to 3.5 T. The coils are cooled to an operating temperature of 4.5 K by liquid helium.

The shape of the coils was designed to create a field that increases near the center, which provides the desired resolution as a function of θ .

The purpose of the magnetic field is to curve the tracks of charged particles without changing their azimuthal (ϕ) angle. This curvature allows for the increased capability of particle identification. Its open structure allows for long path lengths for both charged and neutral particles, which also contributes to particle identification through time-of-flight measurements.

3.2.2 CHERENKOV COUNTERS

When a charged particle moves through a dielectric¹ with a speed greater than the phase velocity of light in that medium, electromagnetic radiation (*i.e.* light) is emitted. This is known as Cherenkov radiation. By changing the refractive index of that medium, the threshold for emission of that light is modified. This effect allows for the distinction of particles otherwise having the same energy and momentum. By using a material with a specific refractive index, a heavier particle may not produce Cherenkov light, but a lighter particle may.

CLAS12 contains two detectors that exploit this Cherenkov effect. The High Threshold Cherenkov Counter (HTCC seen exploded in Fig. 10) is between the solenoid and the first region of the Drift Chambers. It discriminates electrons and pions by being filled with CO₂. This gas has an index of refraction $n = 1.00041$, which forces pion above 4.6 GeV to produce light. If the particle has an energy below this threshold and it produces light, it is an electron.

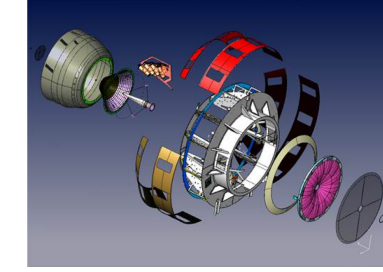


Fig. 10: The High Threshold Cherenkov Counter.

The other Cherenkov detector is the Low Threshold Cherenkov Counter (LTCC), which sits between Region 3 of the Drift Chambers and the Forward Time of Flight detector. It is filled with C₄F₁₂, which allows for the discrimination of pions and kaons at the 2.6 GeV where only pions produce Cherenkov light.

¹A dielectric is any insulator that can be polarized when an electric field is applied.

3.2.3 DRIFT CHAMBERS

There are three regions of Drift Chambers (DC) that collectively allow for the reconstruction of charged particle trajectories. The first region is located in front of the Torus Magnet out the reach of the field. Region 2 is between the coils in the high field region. The third region is after the Torus, but feels a small magnetic field from the coils. Each region is made of six triangular sectors, which are made of small wires and filled with a gas mixture that exploits the process of ionization.

Within the sectors of the DC there are hundreds of wires, half of which are positive and the other half negative. When a charged particle travels through the gas mixture (90% Argon 10% CO₂ for the case of the CLAS12 DC), it knocks off electrons from the gas molecules as it passes. This process is known as *ionization*. In the DC, these ionization electrons that are created as charged particles pass through are accelerated to the nearest positive wire from the electric field created by the negative-positive wire pairs. The ion created is accelerated toward the nearest negative wire by the same electric field.

Using the signals created by the electron-ion pairs as the charged particle travels through the regions of the DC allows for the reconstruction of that particle's path. This information lends itself to the reconstruction of the particle momentum as well as its vertex (*i.e.* where the particle collision occurred). This information will be vital in BONuS12 for identifying the electron created in the $eD \rightarrow e'p_sX$ process.

3.2.4 FORWARD TIME OF FLIGHT

Two charged particles having the same momentum will travel at different speeds depending on their mass. The Forward Time of Flight detector (FTOF) will measure the time of arrival of those charged particles emerging from the target. Primarily, the FTOF will help separate between pions and kaons for energies below 3 GeV. Higher energies are handled by the Cherenkov counters. Because higher momentum particles scatter at lower angles, the FTOF was constructed to have better timing resolution at lower angles. That resolution can be as small as 80 ps at the more forward angles and 150 ps at larger angles (*i.e.* over 35 degrees).

The FTOF is made of six sectors of plastic scintillators coupled to double-sided PMT readout. Within each sector, there are three arrays of counters. Panel 1a, which covers 5 to 35 degrees in θ contains 23 counters. Panel 1b also covers angles

between 5 and 35 degrees and contains 62 counters. Finally, Panel 2 has 5 counters covering only angles between 35 and 45 degrees.

3.2.5 ELECTROMAGNETIC CALORIMETER

Electromagnetic calorimeters measure the energy of particles traveling through it that interact via the electromagnetic interaction. The EC in CLAS12 contains three layers. The preshower calorimeter (PCAL) is the first layer and is used to identify two close gammas, which will help discriminate between neutral pions and single gammas. The next two layers are the inner and outer electromagnetic calorimeters (IC and OC, respectively). Both are used collectively with the PCAL to identify electrons, photons, $\pi^0 \rightarrow \gamma\gamma$, and neutrons.

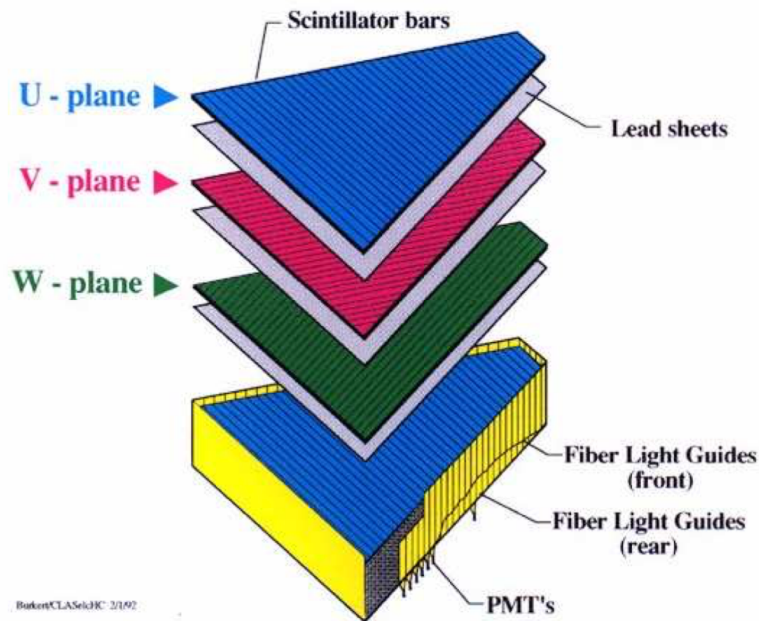


Fig. 11: Exploded view of a sector of the Electromagnetic Calorimeter (EC) for CLAS12. [2]

The requirements of the EC are to identify the electrons with energies above 0.5 GeV, and measurements of photons above 0.2 GeV helping to reconstruct π^0 and η particles through their neutral decays. The EC can also provide photon/neutron separation by utilizing TOF information available.

Each layer of the EC is comprised of six triangular sectors. Each sector is made of alternating layers of scintillators strips and lead sheets. The spatial-coordinate

readout comes from the three planes (U, V, and W) seen in the exploded view of one sector in Fig. 11, which each contain 36 scintillator strips that run parallel to one side of the nearly equilateral triangular sectors. Strips are rotated by 120° in each successive layer, which allows for effective translation to x, y, and z coordinates.

3.2.6 SOLENOID MAGNET

The solenoid magnet and the remaining two detectors to follow (*i.e.* the Central Time of Flight and Radial Time Projection Chamber) are all members of the group known as the Central Detector. The Solenoid is a super-conducting magnet cylindrical in shape that surrounds the beam line. It is capable of producing a field of up to 5 T along the beam line. Charged particles experiencing this field curve in a helical trajectory, which allows for reconstruction of those trajectories and discriminates between charged and neutral particles.

The other purpose of the solenoid is to shield the Forward Detector from electron-electron collisions, called Møller electrons. Because the field is strongest closest to the target, most Møller electrons originating from the beam line are isolated by the solenoid's field to small polar angles (θ) where none of the FD materials exist. The other means of protection from these Møllers comes from a shield around the beam line located just after the Central Detector as well as a shield just in front of a small detector called the Forward Tracker, which for the BONuS12 Experiment will be turned off.

3.2.7 CENTRAL TIME OF FLIGHT

The Central Time of Flight (Fig. 12), just as the FTOF, measures the time of flight of particles originating at the reaction vertex. It is made of 48 scintillator bars that form a barrel and spans polar angles of 35° to 125° that surround the target with full azimuthal coverage. The scintillators are coupled on each end by magnetic-field-sensitive PMTs, which are positioned out of the solenoids field by long light guides. The resulting CTOF operates with a time resolution of 60 ps, which was the requirement for particle identification.

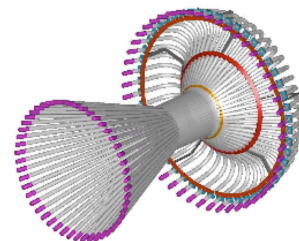


Fig. 12: The Central Time of Flight Detector.

3.3 BONUS12 RTPC

During Run Group F (RGF) in Hall B at JLab all of the detectors just described will be present in addition to one more that will be located inside the solenoid magnet whose outer limits end just before the CTOF. That detector is the BONuS12 Radial Time Projection Chamber (or RTPC). Its purpose is detect protons by way of ionization electrons created as protons pass through the RTPC.

3.3.1 COMPONENTS AND THEIR PURPOSE

Accelerated electrons that enter Hall B hit the RGF target. That target measures 3 mm radially is filled with gaseous deuterium at 7 atm pressure surrounded by a 65 μm thick Kapton wall. When an electron collides with the neutron in a deuteron atom, it continues in the forward direction into the Forward Detector of CLAS12. That collision also results in the ejection of a proton that drifts radially outward into the RTPC.

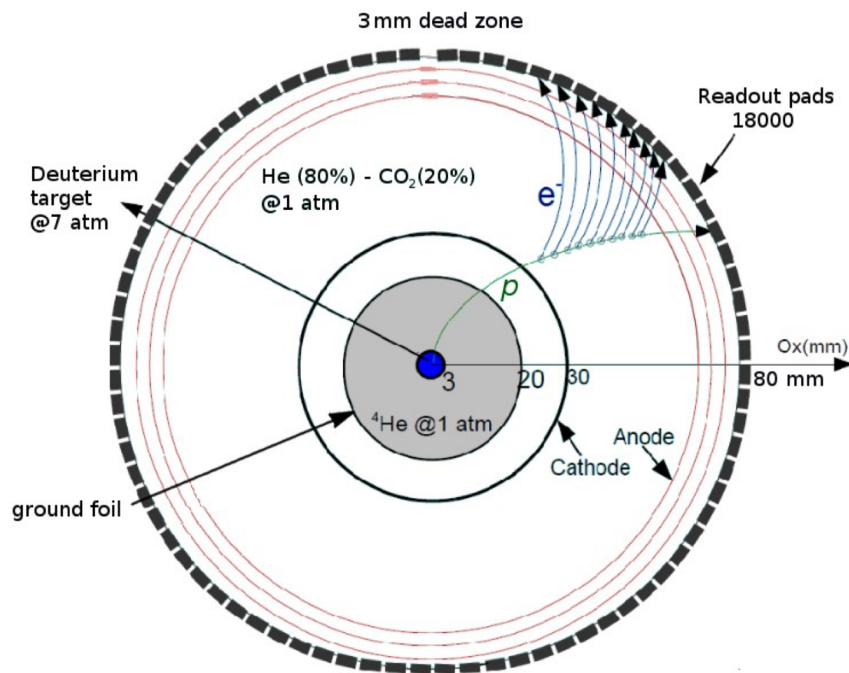


Fig. 13: Cross section of the RTPC showing a proton traversing the detector with ionization electrons drifting toward the readout pad board.

That proton is guided toward the outer edge of the RTPC by way of an electric field created within it. That field is established with a ground foil at 2 cm and a

cathode foil at 3 cm (see Fig. 13). The cathode foil is given a high negative potential and the ground foil is inherently at zero potential. This potential difference creates that electric field through the active region of the RTPC, which begins at the cathode foil and ends at the first Gaseous Electron Multiplier (GEM) foil.

This active region is where the proton will create ionizations along its path outward. This region is filled with a gas mixture of 80% Helium and 20% CO₂, which was chosen for its fast drift times and minimal drift angle (more about this in Section 4.3.4). Because of the magnetic field created by the solenoid, the proton curves in one direction as it moves outward while the ionization electrons it creates curve in the opposite direction due to their opposite charge.

Every time an ionization electron is created, it is also driven by the electric field toward the outer edge of the RTPC where readout pad board waits for its arrival. However, because a single electron cannot be easily readout, that electron will encounter three layers of GEM foils at 7 cm, 7.3 cm and 7.6 cm. Those GEMs are used to amplify the number electrons from one to something significant enough to register on the electronics. Each GEM has a gain of about 100, which means that through three GEM layers, one electron could become 10,000 after exiting the last layer.

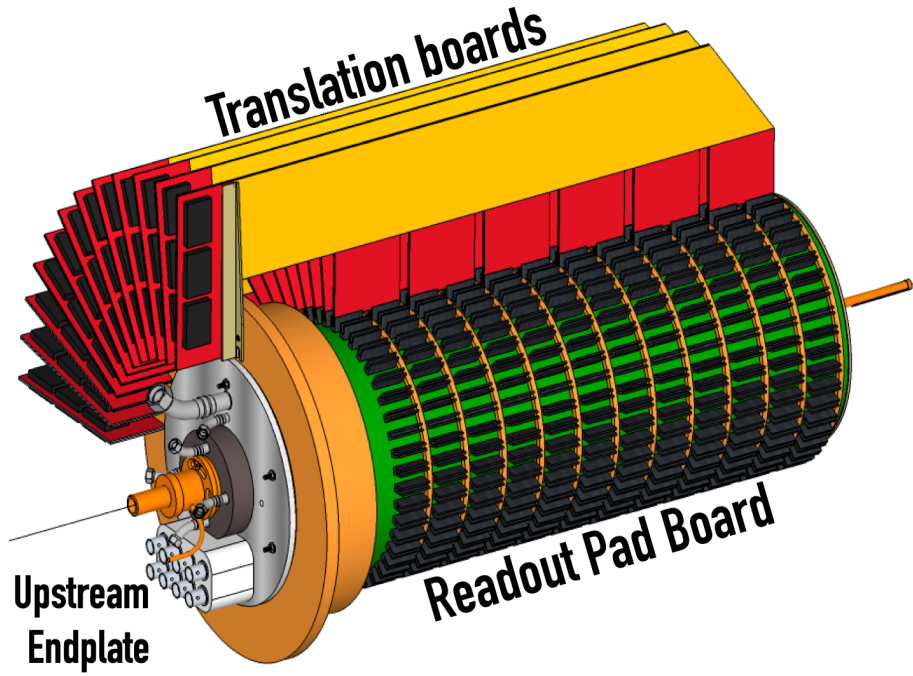


Fig. 14: Design of the RTPC with only one-quarter of the translation boards attached.

Once this avalanche of electrons has been created by the GEMs, their final destination is the read out pad board at 8 cm. The pad board has 180 pads around ϕ by 96 pads in z totaling 17,280 readout pads. These pads, coupled to translation boards that act as current-limiting adapter boards, read the signal that the electron avalanche makes. The electronics then drives the signal to the data acquisition system, which stores the data for analysis.

3.3.2 BONUS12 RTPC DRIFT-GAS MONITORING SYSTEM

The drift velocity of electrons in the RTPC is very sensitive to fluctuations in the gas-mixture and potential, as well as the temperature and pressure of the gas in the active region (see 4.3.4). Therefore, a system was designed that monitors the drift velocity of electrons in the gas mixture of the active region in the RTPC. To achieve this, a small drift chamber was designed whose gas mixture would come from downstream of the RTPC.

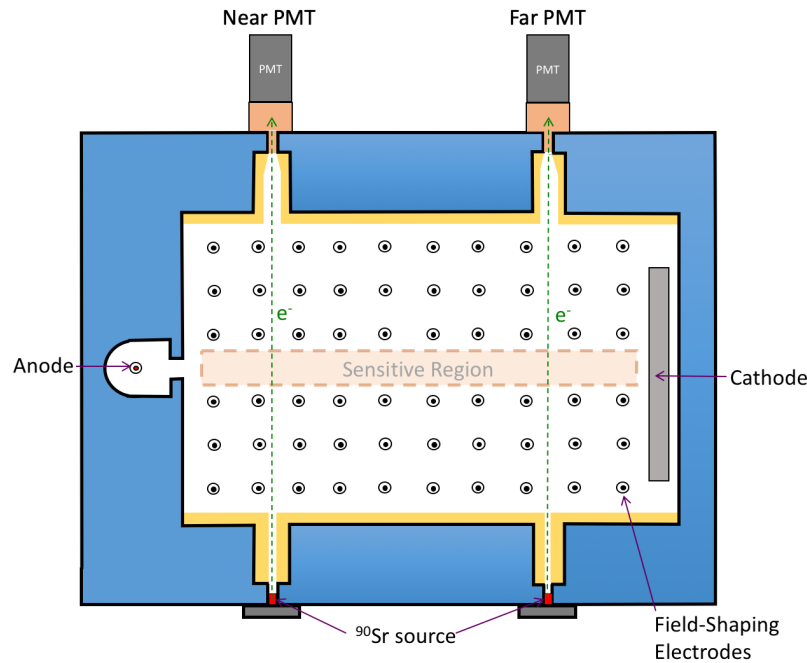


Fig. 15: Design concept of the Drift-gas Monitoring System (DMS) for the BONuS12 Experiment.

Since the purpose of this Drift-gas Monitoring System (DMS) is to measure the drift velocity within the gas mixture, the focus of the DMS design was measuring that velocity through a near-constant electric field. The design concept (seen in Fig.

15) is a drift chamber where two sources at a known distance between them emits β electrons up to associated scintillator/photomultiplier tubes (PMTs). When these electrons travel through the gas, they create ionization electrons along their path. Within a sensitive region in the center of the DMS, those ionization electrons are guided to an anode wire behind a small slit in a grounded plate by an electric field.

The electric field that guides the ionization electrons to the anode is created by a cathode with a high negative potential, an anode with a high positive potential, and field-shaping electrodes that have potentials stepped down by equal amounts from a voltage-divider circuit. This ensures the field within that sensitive region is uniform, so no unwanted acceleration of electrons occurs between the two sources.

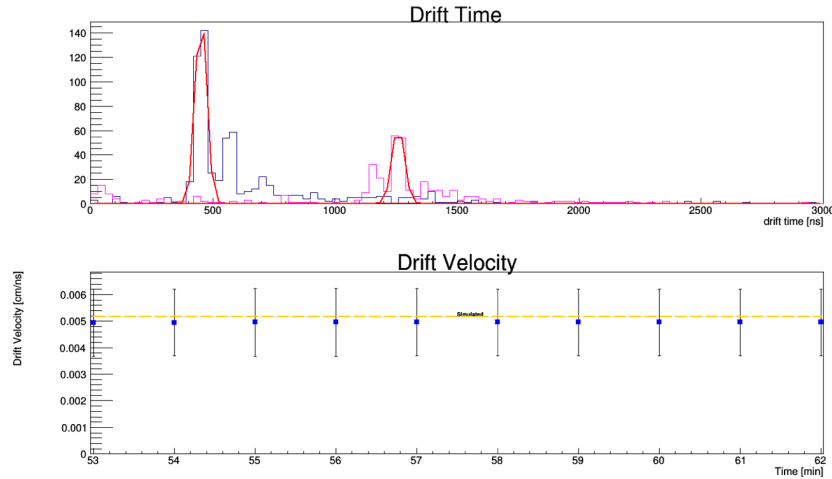


Fig. 16: Monitoring output of the DMS.

When a source β electron is detected by either PMT, a Time-to-Digital Converter (TDC) looks for an associated ionization electron at the anode. When a signal on the anode is seen, the TDC adds that drift time to a histogram. As enough statistics populate the histogram, two peaks are formed from the drift of electrons from the two sources and then a difference in the two times can be calculated. Given the known distance between the sources and the time difference between the two peaks, the drift velocity is calculated. Then the drift velocity is plotted versus elapsed time, giving a means to monitor that velocity (see Fig. 16 for those plots from DMS testing).

3.3.3 CONSTRUCTION AND INTEGRATION

The construction of the BONuS12 RTPC began at Hampton University in Hampton, Virginia around 2017. Because of the cylindrical shape of the detector, mandrels were used widely in the shaping of the detector components. The ground foil, cathode foil, the three layers of GEM foils, and pad board were all assembled using mandrels. Fig. 17 is a drawing of the assembly station for the RTPC, which includes an actuator that removes wrapped foils from the mandrel and places them into the detector on the assembly station.

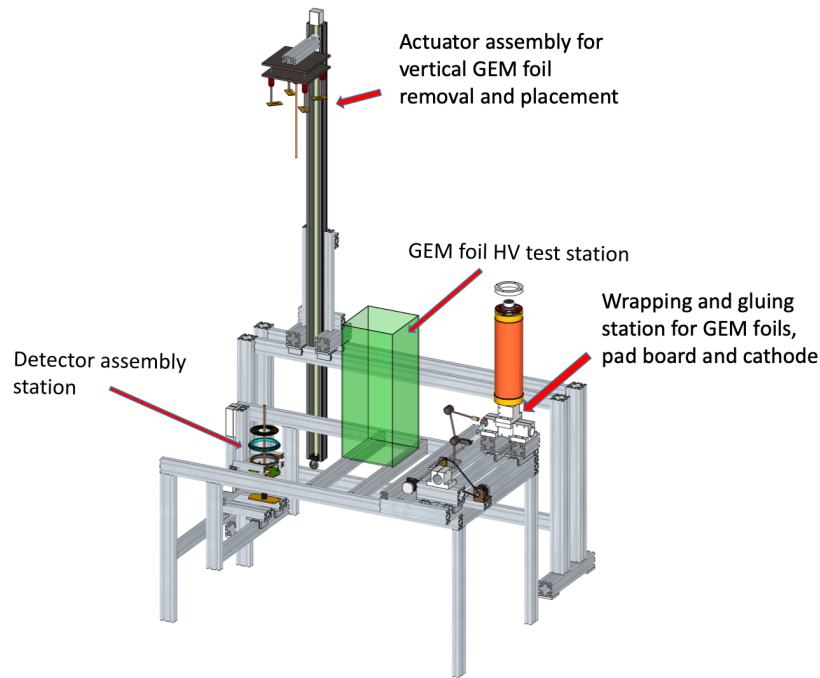


Fig. 17: Assembly station for the RTPC.

The first assembled detector was delivered to JLab in November 2019. The Drift-gas Monitoring was also delivered to JLab in November 2019. Both are undergoing testing in the Experimental Equipment Lab (EEL) with the full array of components that will be installed in the Experimental Hall (*i.e.* RTPC, gas panel including the DMS, DAQ, etc). Once that testing is complete, in late January 2020 the BONuS12 RTPC will be installed in Hall B. Run Group F, of which the BONuS12 Experiment is a part, will also require the installation of three layers of the Forward Micromegas Tracker, switching the Forward Tagger to the FTOFF Møller Shield, as well as cabling for all of those installed detectors. Once this is complete, cosmic ray testing will

begin. This will allow for the first data stream of the RTPC from within the CLAS12 Data Acquisition System whilst inside the hall. Then on 12 February 2020, Run Group F will begin and BONuS12 will begin taking data.

CHAPTER 4

SIMULATION AND DEVELOPMENT

The simulation and development of the BONuS12 experiment has been ongoing essentially since the original BONuS6 experiment in the early 2000's. The goal of BONuS has always been to detect low momentum spectator protons in coincidence with scattered electrons at high Bjorken-x. This is the purpose of the simulation and development (*i.e.* to optimize a detector that will result in high statistics in the relevant kinematic range).

This chapter will focus on the methods used in that detector optimization in preparation for the BONuS12 experimental run. It will cover simulations done to improve geometry, determine electron drift time, and understand energy loss through detector components. The chapter will also go over the construction of the detector. Finally, the process of reconstruction will be covered, which is the way we ultimately determine the kinematics of each event in order to recover the structure functions we are interested in.

4.1 GEANT4 MONTE CARLO (GEMC)

Much of the simulations done in preparation for and during CLAS12 experiments use the Geant4 Monte Carlo (GEMC) software developed by Maurizio Ungaro at Jefferson Lab. GEMC, as the name indicates, uses a toolkit called Geant4. Geant4 was developed by CERN. It was released as a successor in the GEANT software toolkit series, first released in 1998. Since then Geant4 has involved an international collaboration of contributors and maintainers with applications ranging from nuclear physics to medical physics.

The purpose of the Geant4 toolkit is to simulate the passage of particles through matter. This can mean anything from particles going through biological material (*e.g.* simulating the effects of radiation on human tissue) to simulating particles moving through detectors, which will clearly be of much interest to us here. In order to understand how the BONuS12 experiment simulations were conducted with GEMC, first we must become a little more familiar with Geant4.

Geant4 uses the object-oriented programming language C++ in various facilities to exploit its features. The first defining characteristic of this toolkit is its ability to define geometry, or physical layout, of an experiment. This lets us consider how this geometry effects the particles moving through the materials in the experiment. The path that these particles takes as well as the interactions with the materials they pass through is another facility in Geant4 known as tracking.

The Geant4 Monte Carlo (GEMC) is a C++ framework that utilizes Geant4 and the Monte Carlo method of randomized sampling in order to obtain particle behavior through materials. At a very basic level, GEMC can define particle momenta and angles as well as detector geometry and material in order to understand the particle's behavior in that material. One can define a variety of output variables of interest in these simulations like total energy deposited, position, or momentum. There is much more that can be done with this simulation platform that will be discussed through the following sections. First, we must go over one more tool that was used for simulations called Garfield++.

4.2 GARFIELD++

While Geant4 and GEMC both deal well with the simulation of particles' interaction with matter, the particles of interest in the BONuS12 experiment also go through gases and will be under the influence of electric and magnetic fields. For a more specialized simulation of charged particles in such gases with electric and magnetic fields, we use a toolkit called Garfield++, which was developed at CERN. This is extended version of the original Garfield platform that incorporates MagBoltz in the C++ language. MagBoltz solves the Boltzmann transport equations for electrons in gas mixtures under the influence of electric and magnetic fields. This allows Garfield++ to simulate electrons traveling in a gaseous medium under the influence of electric and magnetic fields. The other programs utilized to create a mesh of the RTPC and solve the electromagnetic equations inside the RTPC are GMSH and ElmerSolver, respectively. These packages and their purpose will be described more in the discussion of drift electrons as well as gas-mixture optimization.

4.3 BONUS12 RTPC SIMULATIONS

Throughout the next section, we will focus on the simulations that shed light on particle behaviors in the detector, drove optimization efforts, and offered insight

about expected results. We'll go over all the tools that were used for the simulations and how each one was utilized and implemented. Computer simulations are immensely powerful and tend to be much less expensive than physical exploration and experimentation. We'll discuss how the packages already presented can come together to simulate the entire BONuS12 Experiment from the RTPC to its inclusion in the CLAS12 detector.

4.3.1 GEOMETRY & MATERIALS

The first thing to do when simulating the BONuS12 RTPC in GEMC is to define its geometry and materials. This is done via Perl file, where one can use predefined materials from Geant4 (*e.g.* G4_KAPTON for Kapton, G4_Cu for copper, etc.) or define your own materials. Geometries are defined both in Geant4 and GEMC by solid types like "tube", "box", "sphere", etc. Since the BONuS12 RTPC is made of several different cylinders, most of the geometry definitions are of type "tube". Therefore, we specify the dimensions in terms of r , ϕ and z . For example, the drift volume is defined in the code by

```
$detector{"name"} = "sensitive_drift_volume";
$detector{"mother"} = "rtpc";
$detector{"description"} = "Sensitive drift volume";
$detector{"color"} = "ff88994";
$detector{"type"} = "Tube";
$detector{"dimensions"} = "$rmin*mm $rmax*mm $z_half*mm $phistart*deg
$pspan*deg";
$detector{"material"} = $mate;
$detector{"style"} = 1;
$detector{"sensitivity"} = "rtpc"; ## HitProcess definition
$detector{"hit_type"} = "rtpc"; ## HitProcess definition
print_det(\%configuration, \%detector);
```

where the material (`$mate`) is made of 80% ${}^3\text{He}$ and 20% CO_2 in this case (defined elsewhere) and `$rmin= 30.0`, `$rmax= 70.0`, `$z_half= 192.0`, `$phistart= 0.0`, `$pspan= 360.0`. One defines the units within the declaration of `$detector{"dimensions"};` `$rmin*mm` would be 30.0 mm, for example. There are other variable names that you see within the detector attributes above that are important to understand. The

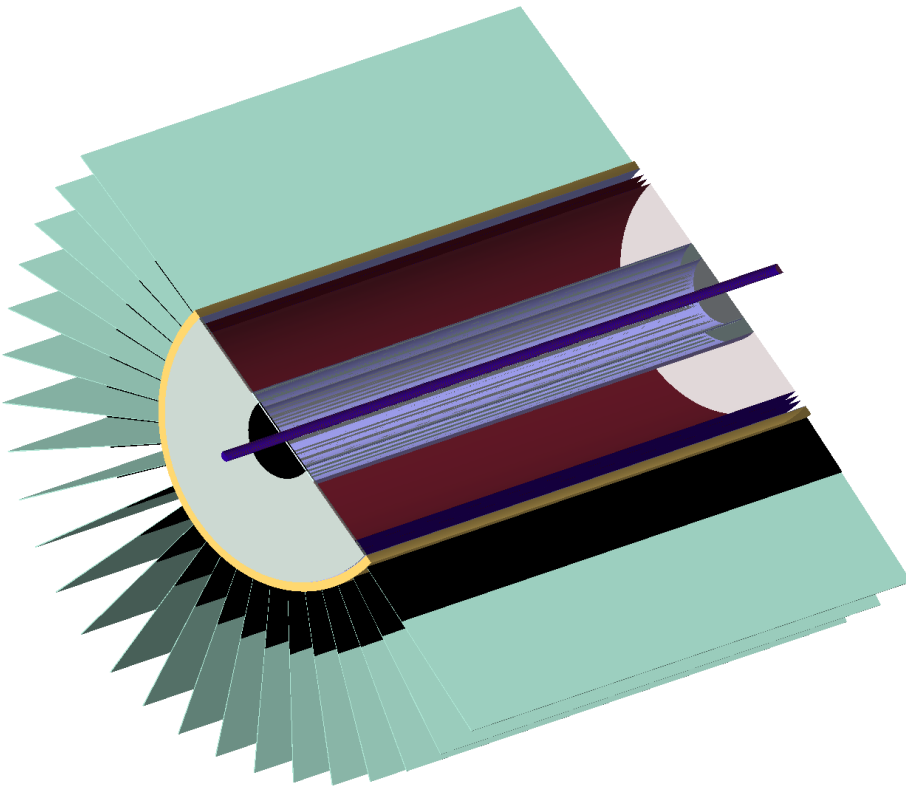


Fig. 18: BONuS12 RTPC geometry implemented in GEMC

variable `style` describes whether the type is a solid (`style = 1`) or wire frame (`style = 0`). The `sensitivity` variable directs GEMC to add the output of this region to the correct bank in the output file. In order to define what particle-interaction output variables appear in the output file for the given volume, we use the `hit_type` variable. Hit type will be covered more in Section 4.3.3 when we discuss what to do when ionization occurs in the drift region.

Not all of the RTPC details can be implemented into GEMC, so we only include the important components in the GEMC simulation. Those components include the main detector parts like the target, ground and cathode foils, GEM foils, and readout pad-board. Then there are the components that had to be included in order to understand their effect on the particles that may be traveling through them (*e.g.* down-stream end plate, electronics and translation boards, support ribs and spines,

etc). Most of these secondary components had to be simplified in order to save time during the simulation process. For example, a cylindrical volume of average density was included outside of the readout pad-board. This density included a proportional amount of the support ribs and spines, electronics, and air. The final geometry can be seen in Fig. 18, which shows half of the RTPC in order to see the internal structure.

Once the geometry is set up for the RTPC, it must be inserted within the CLAS12 detectors in GEMC. The file that brings all these detectors together in GEMC is an XML (*i.e.* extended markup language) file called a *gcard*. This file is where one defines not only which detectors to include in the simulation, but also what variables to include in the output file and what the incoming particle beam should be (*e.g.* momentum, angle, spread, etc.). For example, if one desired 10.6 GeV/c electrons to travel at 0° scattering angle θ and 0° around ϕ , with a spread of ± 10 MeV/c in momentum, $\pm 10^\circ$ in θ and $\pm 180^\circ$ in ϕ , the code would be:

```
<option name="BEAM_P" value="e-, 10.6*GeV, 0.0*deg, 0.0*deg"/>
<option name="SPREAD_P" value="10*MeV, 10*deg, 180.0*deg"/>
<option name="BEAM_V" value="(0, 0, 0)cm"/>
<option name="SPREAD_V" value="(0.3, 20)cm"/>
```

Notice that in this code snippet, the vertex of the particle `BEAM_V` is set to zero and there is a spread on that vertex `SPREAD_V` of $0 \text{ cm} \leq r \leq 0.3 \text{ cm}$ and $-20.0 \text{ cm} \leq z \leq 20 \text{ cm}$), which spans the diameter and length of the BONuS12 RTPC target.

This method of generating particles makes use of GEMC's internal event generator. The particles that can be generated make use of the Geant4 particle bank. The trouble with this internal generator is that we don't have access to multiple particles that we may want to examine (*i.e.* secondary particles). For that we have to look toward another method of generating particles and how to import that file into GEMC.

4.3.2 EVENT GENERATOR

For the purpose of our GEMC simulations in BONuS12, we are primarily concerned with the reaction $eD \rightarrow e'pX$ and so we need a means of generating such events. For that we use an external particle generator called Pythia. Pythia is a program for generating high-energy physics events, which is precisely what we need. It uses theory and models on collisions between particles like e^- , e^+ , p and \bar{p} (*i.e.*

anti-proton) to generate output in a file format name Lund, after the University where the program was developed.

TABLE I: Lund file header

Column	Quantity
1	Number of particles
2	Mass number of the target
3	Atomic number of the target
4	Target polarization
5	Beam Polarization
6	Beam particle type
7	Beam energy (GeV)
8	Interacted nucleon ID (proton or neutron)
9	Process ID
10	Event weight

This Lund output file format has very specific variables that we can take advantage of in GEMC. The first line of this Lund file contains header information for the particles to follow from the collision simulation. This header contains 10 different columns, listed in Table I. The items in bold are used by GEMC. Given the number of particles listed under column 1, there will be a list below the header with particle details for each (see Table II). That is, if there is a 5 listed under the first column in the header, then below the header will be 5 lines for each of the particles. For a simulation with multiple events, subsequent events appear after the last particle of the previous beginning again with the header line.

For the BONuS12 experiment, the event generator created a Lund file with various electron-proton deep-inelastic collisions that we must run through GEMC. To do this, instead of utilizing the GEMC internal event generator, we include the following line of code

```
<option name="INPUT_GEN_FILE" value="LUND, even_gen.lund"/>
```

in the gcard that we use to give direction to GEMC. This file will serve to instruct GEMC how many particles are in each event and the type of particle, its momentum and its vertex. For our purposes in BONuS12, we have Lund files with primary

TABLE II: Lund particles

Column	Quantity
1	Index
2	Lifetime [nanoseconds]
3	Type (1 is active)
4	particle ID
5	Index of the parent
6	Index of the first daughter
7	momentum x [GeV]
8	momentum y [GeV]
9	momentum z [GeV]
10	Energy of the particle [GeV]
11	Mass of the particle [GeV]
12	vertex x [cm]
13	vertex y [cm]
14	vertex z [cm]

electron-proton events that also have a number of additional protons that serve as background. The number of these background protons can vary, but the intent is always to best represent what we would expect to see. Once we run this file through GEMC with all the other variables defined that have been previously discussed, we need to take a look at what happens in the simulation when these protons travel through the RTPC.

4.3.3 DRIFT ELECTRONS

When protons travel through the sensitive region of the RTPC, they ionize the gas creating what are known as ionization electrons. Because of the electric field within that sensitive region, those ionization electrons drift toward the outer edge of the RTPC to the readout electronics. The other thing that happens to protons traveling through the RTPC is that they bend in a helical pattern because of the magnetic field. The ionization electrons that are created also bend, but in the opposite direction of

the protons because they are oppositely charged.

By how much these charged particles bend when moving through the magnetic field created by the solenoid magnetic depends, in part, on the magnitude of that field throughout their path. Therefore, it is very important to get an accurate map (*i.e.* the magnitude and direction of the field at small steps in space around the magnet) of that magnetic field. This is important for both the generation of simulated data and the reconstruction of real data. For the simulated data, the field map will define the path of both protons and ionization electrons within GEMC. For the real data, it will play a role in the reconstruction of kinematics from events.

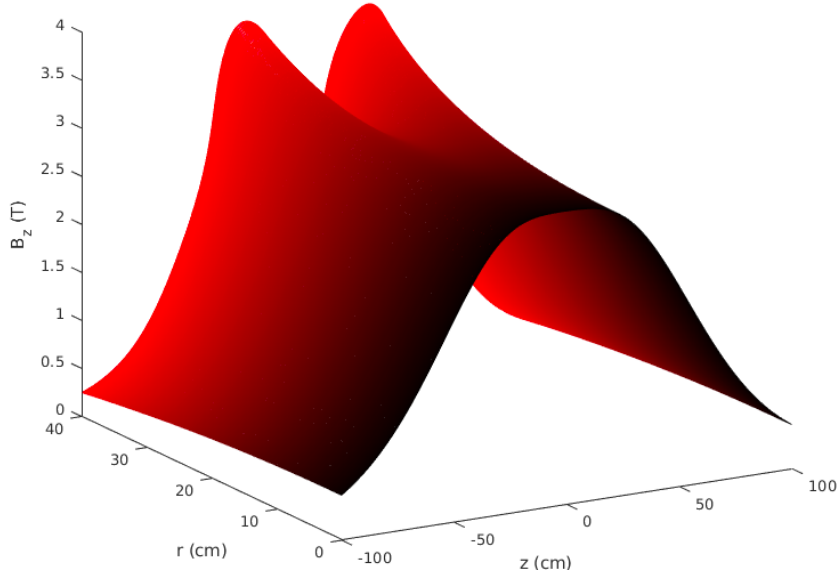


Fig. 19: CLAS12 Solenoid Field Map (V.Lagerquist)

The field map for the solenoid magnet in CLAS12, in which the BONuS12 RTPC will reside, is mapped in steps of z and r (symmetric in ϕ) by Victoria Lagerquist at Old Dominion University (see Fig. 19). Within the sensitive region of the RTPC (*i.e.* $3 \text{ cm} \leq r \leq 7 \text{ cm}$), the map looks like Fig. ?? in steps of z within the RTPC. The map itself takes as input course measurements of the B-field inside the solenoid and finds a more finely-structured field to use in other applications. One of those applications is the simulation of protons traveling through the RTPC.

While GEMC does an acceptable job simulating the proton tracks, Garfield++

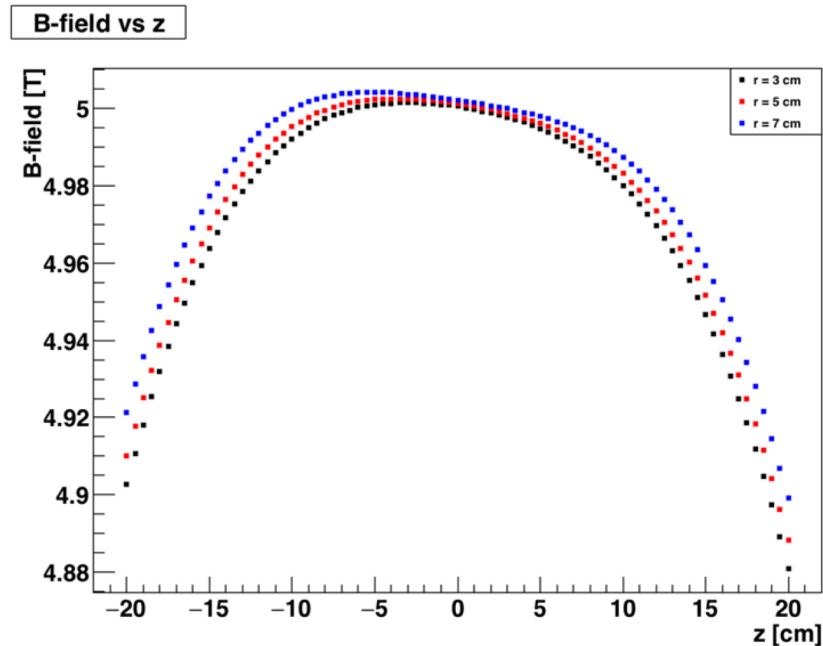


Fig. 20: Magnetic field strength versus z for values of r .

has a more specialized capacity to simulate the ionization electrons (also called drift electrons) created by the protons as they interact with the gas mixture as well as the electric and magnetic fields that are present in the sensitive region of the RTPC. The available build of Garfield++ does not allow for a magnetic field map to be imported, so it had to be written in as a custom feature.

By starting electrons at different values of r throughout the sensitive region (*i.e.* $3 \text{ cm} \leq r \leq 7 \text{ cm}$) and using known values of the electric and magnetic fields, Garfield++ calculated the time it takes that electron to reach the outer edge of the RTPC (*i.e.* 8 cm) as well as the change of angle that it makes. By defining more than one electron for Garfield++ to simulate, we can fit the results to a Gaussian to find the mean and sigma. Those means serve as points in the figures to follow of drift time and drift angle and the sigmas define the diffusion that occurs. As we will see in the coming sections, these drift times and drift angles are of crucial importance to the BONuS12 experiment.

4.3.4 GAS OPTIMIZATION

One of the first uses for the drift time and drift angle from Garfield++ is to

optimize the gas mixture that will be used in the sensitive region of the RTPC. We want a fast drift time to ensure our electronics are able to handle the signal. This would also be less demanding on the trigger and usually means less diffusion. The other property to minimize, drift angle, would ensure that our track is discernible from others in the detector at the same time. Along this line is the need to minimize the diffusion in that occurs within the RTPC in order to increase the resolution of the hits. Thus, we need a gas mixture is that is fast, with small drift angle and diffusion properties, but with a high number of primary ionization events to reconstruct the track.

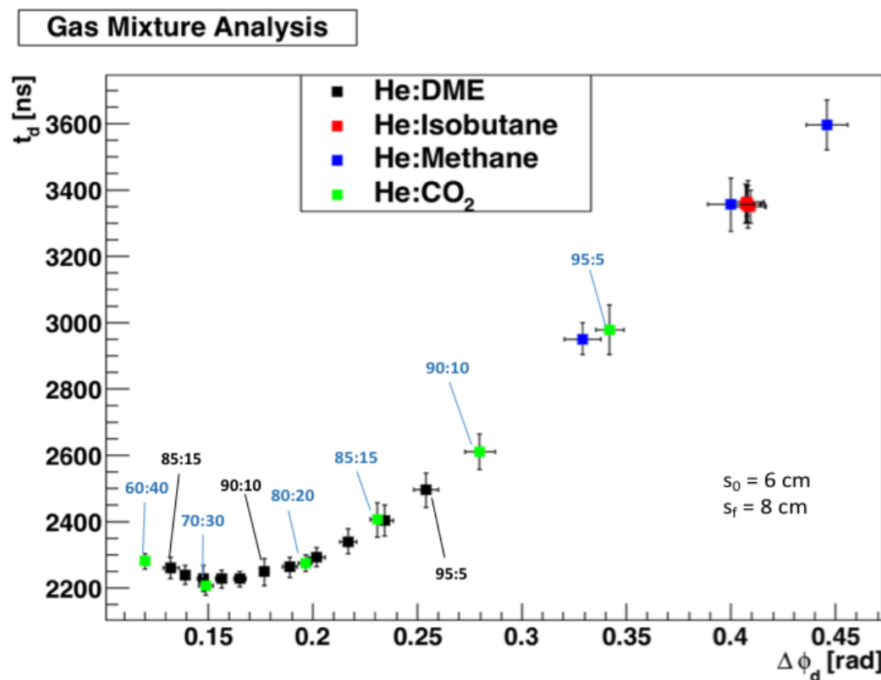


Fig. 21: Drift angle vs drift time for various gas mixtures

The purpose of mixing gases is two-fold. First, there must be a primary gas where primary ionization occurs. Typically this is chosen to be a noble gas such as helium, neon, and argon. A noble gas is usually the primary gas because the outer electron level of the molecule is full, meaning the gas would not interact with the walls of the detector. Also because the outer level is full, the probability of capturing a drift electron is low (i.e. they have a low electron affinity). Second, in order to prevent secondary effects such as photon feedback¹ and field emission², there must exist

¹ Secondary avalanches created from decay through photon emission of excited primary gas atoms.

²Electrons emitted from an electric field.

another gas to act as a quencher. This quencher gas is used to create a stable gas mixture that creates a signal well separated from noise of the electronics.

The first goal is to identify the type of quencher. Fig. 21 shows the drift time as a function of the drift angle of four gas mixtures in a sensitive region containing an electric field of 625 V/cm starting from 6 cm and ending at 8 cm. This electric field corresponds to a potential of -2500 V within the sensitive region, which is high enough to move ionization electrons to the GEMs, but lower than the breakdown potential of the gas (more about this in a few paragraphs). These initial and final radii were chosen to gather results quickly. The error bars on these points are the sigmas of the Gaussian fits of the histogram and represent the diffusion properties of the mixture.

All ratios of He-Isobutane result in almost identical drift angle and drift time. The He-DME starts with a ratio of 85:15 on the far left of Fig. 21 and goes to 100:0 on the far right. The mixture of 87:13 He:DME is at the minimum of the curve. Ideally, as in the original BONuS6 experiment, we could chose this He-DME mixture. However, in an effort to chose a non-flammable gas, we decided to take a look at He-CO₂ mixtures.

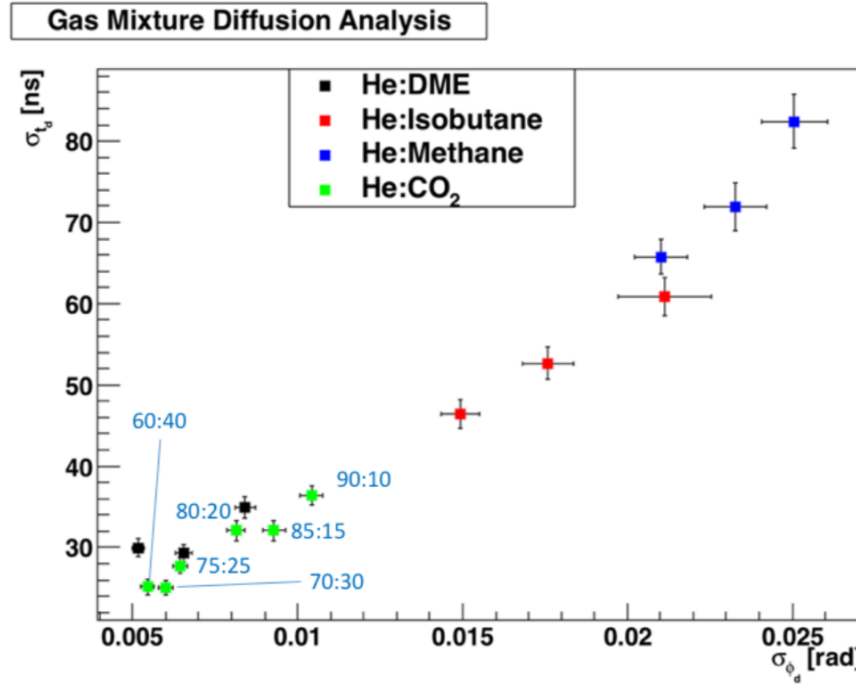


Fig. 22: Diffusion in drift angle vs diffusion in drift time for various gas mixtures

In Fig. 21, the He-CO₂ mixture is in green with the ratios labeled in blue. The

70:30 mixture is at the minimum drift time, which certainly meets the criteria for BONuS12. One of the characteristics that we need to identify during a run is when there may be slight changes in the gas mixture. If we chose to be at the minimum, then identifying when a change occurs would be difficult. This is because while there may be a change in drift angle as the ratio changes, at the minimum there the drift time changes are on the order of nanoseconds. If 80:20 is chosen, then we could more easily identify if a change happens during a run by the noticeable change in both drift angle and drift time. For this reason as well as its non-flammability, the best choice of a gas mixture would be 80%:20% He:CO₂.

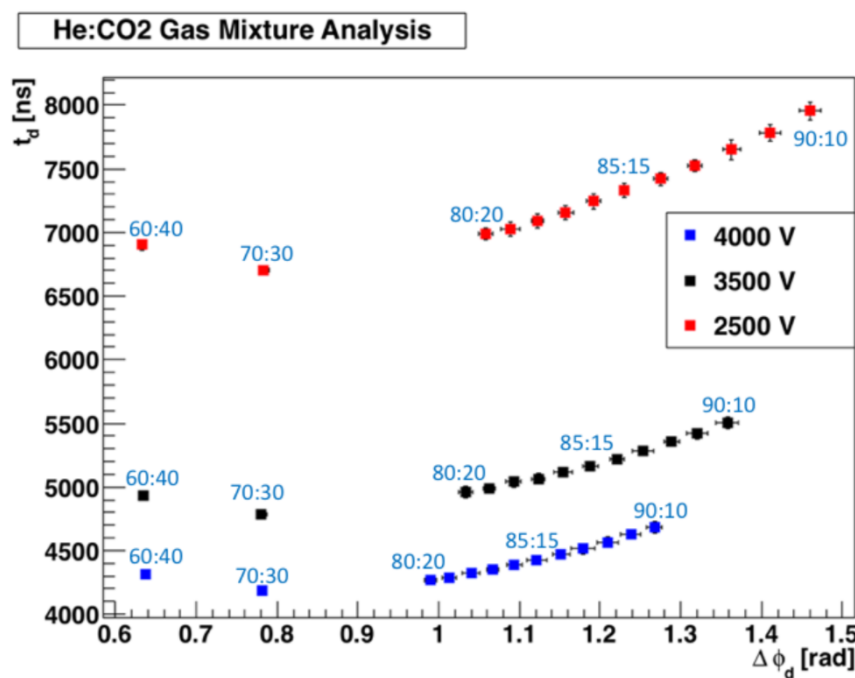


Fig. 23: Drift time versus drift angle for He:CO₂ using various potentials.

Now we must look at reducing diffusion effects for this mixture or at least understand what those effects are for our chosen mixture and potential. If we look at a plot of the diffusion in ϕ (*i.e.* σ_{ϕ_d}) as a function of diffusion in time (σ_{t_d}) as in Fig. 22, we see that the mixtures of He-CO₂ rival those of He-DME for ratios of 80:20-75:25. Given this plot alone, it can be concluded that mixtures below 75:25 of He-CO₂ do better than the He:DME mixtures.

The next step in this optimization is to look at the potential within the sensitive region of the RTPC. Here, note that preliminary experimental studies showed that

the maximum voltage on the cathode would be about -4000 V for He-CO₂. These studies were done with a flat prototype, so if we include that the cathode will be cylindrical, the potential may need to be less. Fig. 23 is a plot of He-CO₂ mixtures for potentials of -2500 V, -3500 V, and -4000 V. Again, the error bars represent the diffusion properties of the mixtures, which comes from the sigma of the Gaussian fit to the histogram. As one would expect, the higher potential, the faster the drift time and the smaller the drift angle.

Given all of this information and the requirements of the detector, we chose a gas mixture of helium-carbon dioxide with a ratio of 80:20 at -3500V. The mixture He-CO₂ meets the requirement of being fast with a small drift angle. For low momentum ions, such as protons in the case of the BONuS12 experiment, reducing multiple scattering is accomplished with low-mass gas mixtures. Thus He-CO₂ is ideal. The CO₂ in the mixture does not serve so much as a quencher, since helium essentially acts as its own quencher, but does limit the diffusion that occurs within the region. In addition, CO₂ is nonflammable.

4.3.5 DRIFT EQUATIONS

By knowing the drift time and drift angles of electrons starting at various values of r and z , we can plot the points and fit the points to an equation. These fit equations can be seen in the plots of t_d vs. r and ϕ_d vs. r (*i.e.* Fig. 24a and Fig. 24b, respectively). We can then use these equations in GEMC to find the drift time and drift angle of a drift electron created at any point along the path of the proton in the sensitive region of the RTPC. In order to speed up simulation efforts, simulation electrons were created at $r = 3$ cm to $r = 7$ cm at 0.5 cm increments and $z = -19$ cm to $z = 19$ cm at 5 cm increments. This give us 81 data points to work with (*i.e.* 9 points per fit line).

The 9 points for each value of z are fit to a second-order polynomial whose coefficients a and b depend on z . This is because the magnetic field changes with z , as shown in Fig. 20, for three values of r that are within the sensitive region of the RTPC. For each of the fit lines, or values of z , we extract the values of a and b for both drift time and drift angle. These values are shown in Fig. 25 and then fit to functions.

The points in Fig. 25 plots are all fit to fourth-order polynomials because of the shape of the magnetic field (see Fig. 20). These extracted functions defining the

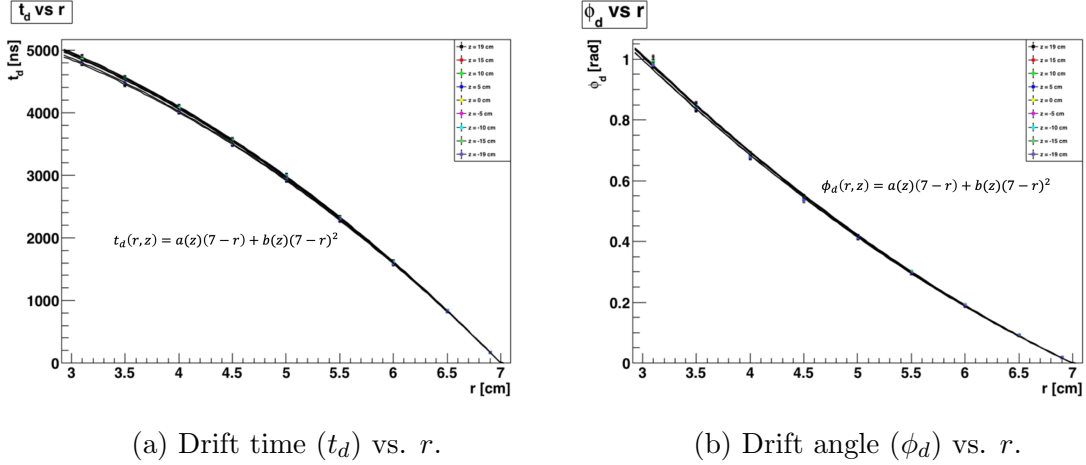
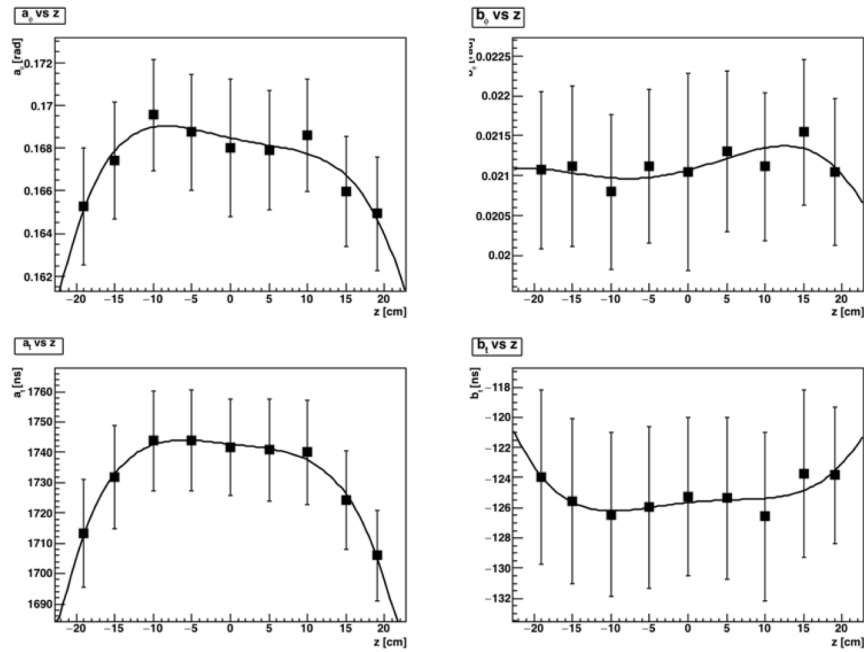


Fig. 24: Plots of drift electron properties.

Fig. 25: Parameters a and b for drift angle (a_ϕ and b_ϕ) and drift time (a_t and b_t).

coefficients a and b for the drift time and drift angle are

$$\begin{aligned}
 a_\phi(z) &= a_{\phi 0} z^4 + a_{\phi 1} z^3 + a_{\phi 2} z^2 + a_{\phi 3} z + a_{\phi 4} \\
 b_\phi(z) &= b_{\phi 0} z^4 + b_{\phi 1} z^3 + b_{\phi 2} z^2 + b_{\phi 3} z + b_{\phi 4} \\
 a_t(z) &= a_{t0} z^4 + a_{t1} z^3 + a_{t2} z^2 + a_{t3} z + a_{t4} \\
 b_t(z) &= b_{t0} z^4 + b_{t1} z^3 + b_{t2} z^2 + b_{t3} z + b_{t4}.
 \end{aligned} \tag{64}$$

These equations go into the `rtpc_hitprocess` class of GEMC. Therefore, when an ionization occurs in the simulation, GEMC uses those equations in Fig. 24b and Fig. 24a to calculate the position of the ionization electron when it reaches the outer edge of the RTPC.

4.4 DMS SIMULATIONS

As we have seen in the previous sections, the drift of the ionization electrons is very sensitive to the gas mixture, temperature, pressure and potential. The Drift-Gas Monitoring System (DMS) had to be designed to measure any fluctuations in those parameters of the gas by way of measuring drift velocity (see Section ??). In order to do that, simulations of the DMS had to be done to optimize the uniformity of the electric field within the drift region as well as the geometry of the chamber itself.

4.4.1 GEOMETRY

The parameters of interest to investigate and optimize were the anode diameter, diameter of the electrodes, and the distances between components. In order to look at these parameters, the geometry of the DMS was implemented into Garfield++, which consisted of its rectangular frame, grounded anode enclosure, anode wire, cathode plate, and field-shaping electrodes.

The first step is to define the gas mixture and geometry of the box used to house all of the DMS components. By using the `Sensor` class in Garfield++, the framework and wires necessary to see the DMS response was built. Then, as seen in the code snippet below, grounded planes were placed along the box.

```
// Setup the gas
MediumMagboltz* gas = new MediumMagboltz();
gas->SetComposition("He",80., "CO2",20.);
gas->SetTemperature(293.);
gas->SetPressure(760.);
gas->EnableDrift();           // Allow for drifting in this medium
gas->PrintGas();

// Build the geometry
GeometrySimple* geo = new GeometrySimple();
```

```

SolidBox* box = new SolidBox(L_x/2., L_y/2., L_z/2., L_x/2., L_y/2.,
    L_z/2.);
geo->AddSolid(box, gas);

// Make a component with analytic electric field
ComponentAnalyticField* comp = new ComponentAnalyticField();
comp->SetGeometry(geo);

// Create a sensor for readouts
Sensor* sensor = new Sensor();
sensor->AddComponent(comp);

// Create grounded planes at the edges of the box
comp->AddPlaneX(0.,0., "x_min");
comp->AddPlaneX(L_x,0., "x_max");
comp->AddPlaneY(0.,0., "y_min");
comp->AddPlaneY(L_y,0., "y_max");

comp->AddReadout("x_min");
comp->AddReadout("x_max");
comp->AddReadout("y_min");
comp->AddReadout("y_max");

sensor->AddElectrode(comp, "x_min");
sensor->AddElectrode(comp, "x_max");
sensor->AddElectrode(comp, "y_min");
sensor->AddElectrode(comp, "y_max");

```

Next, the anode and ground plate surrounding that wire was defined. The following code snippet shows the anode wire defined by a single declaration.

```

// Anode
comp->AddWire(x_0 + r_a + wall_d/2., L_y/2, dAnode, vAnode, "a", 100.,
    50., 19.3);
comp->AddReadout("a");
sensor->AddElectrode(comp, "a");

```

The ground plate surrounding the anode was constructed from a number of large-diameter grounded wires that were placed to form that shape of that plate, since Garfield++ has a difficulties with these rather complicated structures. The same was done for the cathode plate, which used two layers of wire components. The electrode wires were all placed individually, with one example in the code snippet below.

```
comp->AddWire(dist, L_y/2.+b/2.+(i*s_y), dWire, Ex*(s_1 + (j*s_x)), name,
    100., 50., 19.3);
comp->AddReadout(name);
sensor->AddElectrode(comp, name);
```

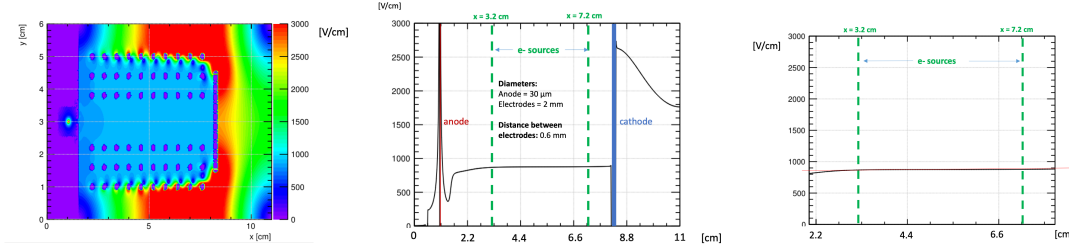
The function `AddWire(double x, double y, double D, double V, string label, double L, double T, double rho)`, places the wire at `x` and `y` with diameter `D`, potential `V`, label of the wire, length `L`, tension `T`, and density `rho` in that order. This placement was repeated 60 times completing 10 rows of electrodes with 6 wires comprising each electrode.

4.4.2 ELECTRIC FIELD

Once the geometries and code were in place, simulations to optimize those geometries were done to optimize the electric field. The primary concern was ensuring near-homogeneity of the electric field within the sensitive region. In order to look at that electric field, we need to look at the field profile along the plane where the anode lies.

Fig. 26a shows the contour map of the field, whose surface contour quantities are on the right legend. The plot in Fig. 26a is made using the `FieldView()` class. The potential from the cathode through to the electrodes was set to mirror what the electric field would be inside the RTPC (*i.e.* 875 V/cm). The profile of the field along the line at $y = 3$ cm is shown in Fig. 26b and Fig. 26c shows a zoom in to between the two sources to ensure its homogeneity (*i.e.* a straight line). These plots are created using the `PlotProfile()` function of the `FieldView()` class.

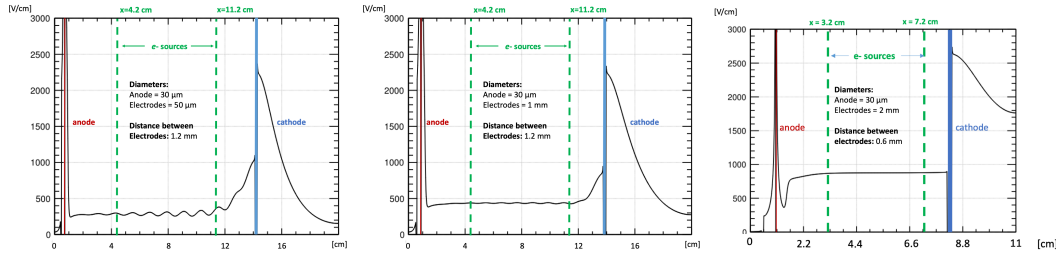
To achieve this straight line indicative of homogeneity, many simulations took place varying the electrode diameter and distance. The progression of these simulations can be seen in Fig. 27, beginning with small diameter electrodes (*i.e.* 50 μm) and a distance of 1.2 mm between each electrode (see Fig. 27a). The small diameter



(a) Electric-field contour map (b) Electric-field profile (c) Zoomed in electric-field along the cross-section in $x-y$ along the plane of the profile to between the two plane. anode. sources.

Fig. 26: Simulations of electric field within the DMS. In the profile plots in (b) and (c), the cathode and anode's locations are denoted as blue and red lines respectively. The sources and PMT's location and subsequent electron beams are pictured as green dotted lines.

coupled with the rather large distance between electrodes creates the large waves of field, which is not at all homogeneous. Fig. 27b shows the field profile with thicker electrodes (*i.e.* 1 mm), but the same separation as Fig. 27a (*i.e.* 1.2 mm). The waves of the field seem to be calmer, but still inhomogeneous.



(a) Electric field profile (b) Electric field profile (c) Electric field profile with electrode separation with electrode separation with electrode separation of 1.2 mm and diameter of 1.2 mm and diameter of 0.6 mm and diameter of 50 μm . 1 mm. 2 mm.

Fig. 27: Simulations electric field profile within the sensitive region of the DMS with various electrode diameters and distances.

Lastly, in Fig. 27c, the electrode diameter was set to 2 mm and the distance between electrodes was decreased to 0.6 mm. The field here in between the sources

is nearly homogeneous. Fig. 26c is zoomed in to that area between sources to verify how flat (*i.e.* homogeneous) the field is there.

Because of these simulations, we were able to identify the frame size, electrode and anode wire diameter, and distances between components. The distance between the cathode and the first set of electrodes was also chosen to be 0.6 mm, which also is the distance from the last electrode to the ground plate.

4.4.3 DRIFT VELOCITY

The last step of the Garfield++ simulations is to determine what we should expect for a drift velocity from the DMS. Just like the physical DMS, the drift velocity is calculated by taking the drift times from ionization electrons created at the lines of the sources that travel to the sources. In the simulations, electrons are started at one of the two areas where the sources would exist. From here the simulation tracks them toward the anode, and a histogram of the drift time is filled.

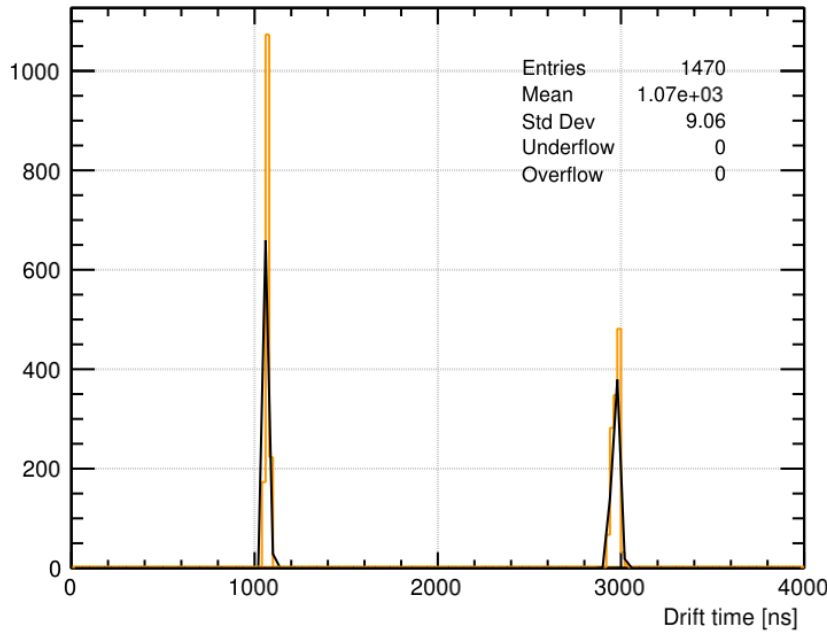


Fig. 28: Simulated drift time for electrons beginning at both the near and far sources from the anode.

Fig. 28 shows the drift times from 20 ionization electrons beginning at locations of both the sources. By taking the means from both Gaussian fits of each collection of drift times with the distance between the two sources (*i.e.* 4 cm), the drift velocity

can be calculated. That drift velocity from Garfield++ simulations is

$$v = \frac{\Delta d}{\Delta t} = \frac{d_f - d_n}{t_f - t_n} = \frac{4 \times 10^4 \mu\text{m}}{2969.90\text{ns} - 1070.75\text{ns}} = 21.06 \mu\text{m/ns}. \quad (65)$$

This gave us an idea what to expect when beginning the data acquisition process.

CHAPTER 5

DATA ANALYSIS

5.1 ELECTRON RECONSTRUCTION

5.2 PROTON RECONSTRUCTION

5.3 HELIX FITTER AND KALMAN FILTER

5.4 CALIBRATION

5.5 CUTS AND CORRECTIONS

5.6 KINEMATIC COVERAGE AND DATA BINNING

5.7 ACCEPTANCE CORRECTION

5.8 ELECTRON DETECTION EFFICIENCY

5.9 BACKGROUND SUBTRACTION

5.10 CROSS SECTION CALCULATION

5.11 RADIATIVE CORRECTIONS

5.12 SYSTEMATIC ERROR EVALUATION

CHAPTER 6

RESULTS

REFERENCES

- [1] C. L. D. Douglas and G. Krafft, “The continuous electron beam accelerator facility: CEBAF at the Jefferson Laboratory,” 2001.
- [2] G. Gilfoyle and K. Sherman, “Geometry update for the electromagnetic calorimeter in CLAS12,” *CLAS12 Note 2014-008*, 2014.
- [3] P. Stoler, “Baryon form factors at high Q^2 and the transition to perturbative QCD,” *Physics Report*, vol. 226, pp. 103–171, 1993.
- [4] F. Halzen and A. Martin, *Quarks and Leptons: An Introductory Course in Modern Particle Physics*. John Wiley and Sons, 1984.

VITA

Nathan M Dzbenksi
Department of Physics
Old Dominion University
Norfolk, VA 23529

TODO: To be updated later!

Typeset using L^AT_EX.